

TALLINN UNIVERSITY OF TECHNOLOGY

Faculty of Chemistry and Materials Technology

Department of Materials Science

Chair of Semiconductor Materials Technology

Surface defects characterization and electrochemical corrosion
studies of TiAlN, TiCN and AlCrN PVD coatings.

Master Thesis

OLASUNKANMI JOHN AJIBOYE

Supervisor: Maksim Antonov, Senior Research Scientist

Chair of Metal Processing

Co-Supervisor: Janis Baronins

Materials and Processes of Sustainable Energetics KAYM09

TALLINN 2016

TALLINNA TEHNIKAÜLIKOOL

Keemia- ja materjalitehnoloogia teaduskond

Materjaliteaduse instituut

Pooljuhtmaterjalide tehnoloogia õppetool

TiAlN, TiCN ja AlCrN PVD pinnete pinnadefektide karakteriseerimine ja
elektrokeemilise korrosiooni uuringud

Magistritöö

OLASUNKANMI JOHN AJIBOYE

Juhendaja: Maksim Antonov, Vanemteadur

Metallide tehnoloogia õppetool

Kaasjuhendaja: Janis Baronins

Materjalid ja protsessid jätkusuutlikus energeetikas KAYM09

TALLINN 2016

Declaration

Hereby, I declare that this master thesis, my original investigation and achievement, submitted for the master degree at Tallinn University of Technology has not been submitted for any degree or examination.

.....

(Author's signature

Table of Contents

List of Figures.....	5
List of Tables	6
Nomenclatures.....	7
Abstract.....	9
Resümee	10
1 INTRODUCTION.....	11
2 LITERATURE REVIEW.....	13
2.1 Surface Degradation of Metal Components.....	13
2.2 Mechanisms of Degradation in Metals	14
2.2.1 Wear and Friction.....	14
2.2.2 Corrosion.....	14
2.2.3 Corrosion of Coating-Substrate Systems	15
2.2.4 Electrochemical Process of Corrosion.....	16
2.3 Surface defects in PVD hard Coating.....	21
2.3.1 Surface Defect Formation in Hard Coatings.....	21
2.3.2 Characterization of surface defects	22
2.4 Coating Deposition Technologies.....	26
2.4.1 CVD (Chemical Vapour Deposition)	28
2.4.2 PVD (Physical Vapour Deposition)	28
2.4.3 TiAlN, AlCrN and TiCN coatings.....	30
3 Materials and Experimental Procedures	33
3.1 Substrate Deposition and Preparation	33
3.1.1 Coating deposition	33
3.2 Evaluation of Coating	34
3.2.1 Measurement of coating thickness.....	34
3.2.2 Compositional and Microstructural characterization	34
3.3 Electrochemical Characterization of corrosion behavior of coatings	35
3.3.1 Operational Procedures	37
4 Results and Discussions	45
4.1 Surface Morphology.....	45
4.1.1 Coating thickness	45
4.1.2 Defects on coatings.....	45
4.1.3 Chemical Composition	49

4.2	Corrosion behavior of coatings	49
4.2.1	Potentiodynamic Polarization Tests.....	50
5	Conclusions.....	56

List of Figures

Figure 2.1: Schematic view of the 3 electrode setup.	18
Figure 2.2: A typical Tafel plot.....	19
Figure 2.3: Classic Tafel analysis	20
Figure 2.4: Planar SEM micrographs of CrN hard coating showing the morphology of typical defects.	24
Figure 2.5: Defect Morphologies:	25
Figure 2.6: Deposition processes of thin hard coatings	27
Figure 2.7: Schematic of the PVD process based on magnetron sputtering.....	30
Figure 3.1: The Platit π 80 deposition system.....	34
Figure 3.2: The SEM Hitachi TM-1000 Tabletop.	35
Figure 3.3a: The Autolab PGSTAT30 galvanostat/potentiostat system.....	36
Figure 4.1: SEM micrograph showing sphere-like macrodroplets on the AlCrN coating.....	46
Figure 4.2: SEM micrograph showing: A nodule-detached crater (open void) on AlCrN coating surface	47
Figure 4.3: SEM image showing: Interconnected cracks on surface of TiAlN I coating.....	47
Figure 4.4: SEM Micrograph Pinhole defect left by ejected particle on TiCN film.	48
Figure 4.5: SEM micrograph showing: Large crater like defects on TiCN surface.	48
Figure 4.6: SEM micrograph of TiAlN II coating	49
Figure 4.7: Potentiodynamic polarization curves of the substrate and coatings.....	52
Figure 4.8: Protective Efficiency of coatings	53
Figure 4.9: Protective efficiency and polarization resistance of the substrate and coatings....	53
Figure 4.10: Corrosion Potential of Substrate and Coatings	55
Figure 4.11: Corrosion current density i_{corr} ($\mu\text{A}/\text{cm}^2$) of the coatings and substrate.....	55

List of Tables

Table 4.1: Coating thickness.....	45
Table 4.2: Results of potentiodynamic polarization tests	50

Nomenclatures

AFM	Atomic Force Microscopy
AISI	American Iron and Steel Institute
AlCrN	Aluminum Chromium Nitride
ASTM	American Society for Testing and Materials
CAD	Cathodic Arc Deposition
CR	Corrosion Rate
CrAlN	Chromium Aluminum Nitride
CrN	Chromium Nitride
CVD	Chemical Vapor Deposition
E_{corr}	Corrosion Potential
EDS	Energy Dispersive X-ray spectroscopy
E_{OCP}	Open-Circuit Potential
EW_{alloy}	Equivalent Weight of Alloy
FIB	Focus Ion Beam
I	Electrode Current
i_{corr}	Corrosion Current Density
LARC	Lateral Rotating ARC-Cathodes
OCP	Open Circuit Potential
PVD	Physical Vapor Deposition
R_p	Polarization resistance
$S_{c,m}$	Mechanical Severity of Contact
SCE	Saturated Calomel electrode
SEM	Scanning Electron Microscopy
TiAlN	Titanium Aluminum Nitride
TiCN	Titanium Carbon Nitride
WC	Tungsten Carbide

β_a	anodic polarization constant (Tafel slope of anodic corrosion reaction)
β_c	cathodic polarization constant (Tafel slope of cathodic corrosion reaction)
μ	Coefficient of Friction (CoF)
RE	Reference Electrode
WE	Working Electrode
CE	Counter Electrode

ABSTRACT

In this research, three different types of coatings have been deposited successfully on AISI 316L steel substrate by a Platit π^{80} system under a reactive nitrogen atmosphere using Lateral Rotating ARC-Cathodes (LARC) technology. The coatings are TiCN, TiAlN and AlCrN. Two different samples of TiAlN coatings with different thickness was evaluated, designated as TiAlN I and TiAlN II (with a coating thickness of 1.5 and 2.4 μm respectively) .The coating thickness of the AlCrN and TiCN are 3.6 and 3.7 μm respectively.

All the coatings were investigated for the presence of surface defects with use of Scanning Electron Microscopy (SEM) imaging. Also the coatings' electrochemical corrosion behavior was evaluated by a potentiodynamic polarization measurement in 3.5% wt. NaCl solution.

SEM images of the coatings showed that all the coatings had one form of defects on its surface. Similarly, analytical evaluation of electrochemical data from the potentiodynamic polarization measurement was used in estimating the porosities of the coatings. The electrochemical data showed that there is a considerable shift in the corrosion potential of the coatings as compared to the uncoated substrate. This is indicative of the fact that all the coatings served as protective covering for the substrate against the corrosive media despite the presence of defects.

Also the evaluation of corrosion current density clearly shows a better corrosion resistance of the coatings. The thicker TiAlN sample (TiAlN II) exhibited the best protective efficiency of 98.68 % and lowest porosity of 0.012 %. The AlCrN showed the least corrosion resistance, protective efficiency and the highest corrosion rate; this could be associated with the nature of defects present in the coating morphology.

Based on the electrochemical data the following order of protective efficiency was established, from best to the worst: TiAlN II (98.68 %) > TiCN II (97.75 %) TiAlN I (81.63 %) > AlCrN (73.76 %). Similarly, the calculated porosity is in the following order, from the highest to the lowest porosity (worst to the best): TiAlN (12.83%) > AlCrN (1.50 %) > TiCN (0.051 %) > TiAlN II (0.012 %).

RESÜMEE

Selle uurimistöö käigus sadestati AISI 316L roostevabaterase alusplaadile edukalt kolme eritüüpi pinnnet kasutades lämmastiku keskkonnas füüsikalise aurustussadestusseadet (PVD) Platit $\pi 80$ (pöörleva kaarleekaurustus katoodiga LARC).

Uurimiseks valiti kolm pinnet: TiCN, TiAlN ja AlCrN. TiAlN pinne oli sadestatud kahe erineva paksusega: TiAlN I – 1.5 μm ja TiAlN II – 2.4 μm . AlCrN ja TiCN pinnete paksus oli vastavalt 3.6 ja 3.7 μm .

Pinnete defekte uuriti skaneeriva elektronmikroskoobi (SEM) abil. Lisaks uuriti ka pinnete potentsiodünaamilist polarisatsioonkäitumist 3.5 % wt. NaCl lahuse elektrokeemilises korrosioonikeskkonnas.

SEM piltidel on näha, et sageli leitakse ainult üks pinnadefekt - pinna sees olevad makroosakesed, kuid esinevad ka praod ja augud. Pinnete poorsus arvutati analüütiliselt kasutades elektrokeemilisi andmeid, mis olid saadud polarisatsioonkäitumise mõõtmisel.

Elektrokeemiliste andmete põhjal selgus, et pinnete korrosiooni potentsiaal on märkimisväärselt kõrgem kui aluspinna oma.

See tõestab, et vaatamata defektide olemasolule on pinded suutlikud kaitsma aluspinnet korrosiooni keskkonnas. Ka korrosiooni voolutihedus näitas pinnete positiivset mõju aluspinna kaitsmisele.

Kõige paksema TiAlN kaitsekihiga (TiAlN II) katsekeha näitas parimat kaitseefektiivsust (98,68 %) ja kõige madalamat poorsust (0.012 %). AlCrN pinne näitas kõige kehvemat korrosiooni kaitseefektiivsust ja kõrgemat korrosiooniintensiivsust, see võib olla seotud pinnete morfoloogiale mõjuvate defektide iseloomust.

Tuginedes elektrokeemilistele andmetele võib pinded järjestada kaitseefektiivsuse järgi (alustades parimast) järgmiselt: TiAlN II (98.68 %) > TiCN (97,75 %) TiAlN I (81.63 %) > AlCrN (73.76 %).

Poorsuse järgi võib pinded asetada pingeritta (alustades kehvemast) järgmiselt: TiAlN I (12.83 %) > AlCrN (1.50 %) > TiCN (0.05 %) > TiAlN II (0.012 %).

1 INTRODUCTION

Most engineering materials are exposed to various types of conditions during their life time. Usually, the working conditions of materials mean that their surfaces are constantly exposed to harsh working environments. This leads to a degradation of the materials surface over time. The impacts of surface degradation are noticeable in the shortened lifetime of the components in which the material is employed, also a reduction in efficiency and sometimes complete failure of materials which leads to occupational accidents.

Generally, materials undergo degradation in the form of wear and/or corrosion. These are the most common type of attacks that degrades the surface of the material [1]. These forms of degradation are considered the major factors that results in most material failures. Various studies opined that majority of the losses caused by corrosion and wear can be minimized by the application of effective coatings. This has led to the rapid development of various hard coating technologies and materials in the past decades.

Surface modification with hard coatings materials helps improve the service life as well as the performance of materials. They provide a wide range of properties that is essential in the optimization of desired functionalities. Transition metal nitrides based hard coatings (e.g. TiN, CrN and TiAlN) have shown incredible capacity to improve the corrosion and wear resistance of various steel substrates [2]. Hard coatings impart desired properties such as low friction, thermal stability, high corrosion and oxidation resistance and high hardness into materials and tools [3].

However, despite the importance of coatings in extending material life span and improving their efficiency and performance they are usually not perfect. Growth defects are present in all types of coatings, especially PVD (Physical Vapor Deposition) hard coatings. They undermine the protective efficiency of the coatings by having a detrimental influence on their tribological properties and corrosion resistance. The presence of defects especially affects the electrochemical behavior; they expose the substrate to direct contact with corrosive media leading to rapid corrosion rates [2]. In order to improve the tribological and corrosion properties of PVD hard coatings it is important to minimize the concentration of growth defects [4].

The primary objective of this thesis is to investigate the effect of surface defects on different types of coatings (namely TiAlN, TiCN, and AlCrN). To characterize how the defects impact their abilities to serve as protective coating for materials in industrial applications such as in dry machining, fuel cells and in biomedical devices. A critical issue of this study is to investigate the coating integrity and study the correlation with the coatings' protective efficiency and corrosion resistance. SEM analyses have been employed in characterizing the nature of defects. Electrochemical characterization of the coatings is performed to investigate their corrosion behaviors in a simulated corrosive environment (3.5 wt. % NaCl solution).

2 LITERATURE REVIEW

2.1 Surface Degradation of Metal Components

All metallic components perform in one environment or another. Often the aggressiveness of the environment in which the material is been used leads to degradation or deterioration of the physical and mechanical properties of the metal or alloy. Surface degradation may take the form of simple appearance loss, or cracking of components which may sometimes lead to catastrophic failure. Material degradation also leads to premature failure of metal components, environmental pollution and they also constitute risk to human lives. The aggressive environment described above includes, but not limited to: atmospheric exposure at ambient temperatures, reactive gases at high temperatures, soil or water, weak and strong chemicals, alkaline and acidic media nuclear radiations etc. [5].

The nature of degradation varies due to the nature of the environmental attacks and nature of force. All degradation is associated with the effects of force and heat, which results in wear and thermal corrosion. Chemical degradation is related to destructive reactions, which causes corrosion [1]. This study intends to analyses surface degradation as a result of physical and chemical degradation mechanisms. It is imperative to understand the nature and mechanism of degradation so as to devise preventive measures against the loss and failures associated with material degradation. This has been the primary reason for the emergence and rapid development of protective coatings over the past decades; to enhance the performance efficiency of metallic components [6]–[9].

According to F. Cai [1] surface damage usually have three consequences which can be summarized as follows: constant loss of material volume and weight, material loss and material gain. Furthermore, weight or volume changes as well as damage can still occur due to structural changes, plastic deformation, and surface cracks. Any of the outlined damages would lead to a deterioration of the desired functions of the metallic components and cause the material to degrade much more rapidly. Hence, it is of utmost importance to protect the surface of metals with materials with superior properties. This will ultimately lead to the enhancement of specific characteristics and performance efficiency.

2.2 Mechanisms of Degradation in Metals

2.2.1 Wear and Friction

According to Bhushan and Gupta [10], wear is a process of removal of material from one or both of two solid surfaces in solid state contact, occurring when two solid surfaces are in sliding or rolling motion together. It results in a progressive loss of material from the solid surface, due to the relative motion between the surface and a contacting substance. The mechanism of wear can be summarily classified as mechanical, chemical and thermal wear; the modes can be further subdivided into abrasive, adhesives, fatigue, corrosive, melt and diffusive wear [11].

There are two major concerns in the classification of wear, namely: the extent of the damage and the wear mechanism. Based on the extent of damage, wear can be classified as mild or severe [12].

The specific wear rate and coefficient of friction are the distinguishing factor between mild and severe wear. The transition from mild to severe wear results in an acceleration of degradation. It is essential to be able to predict the onset of transition from mild to severe wear. This will help to prohibit the transition and thus extend the life time of the components [1]. Adachi et al., [12] has proposed the mechanical severity of contact ($S_{c,m}$) as one of the physical parameters for evaluating the transition from mild to severe wear.

2.2.2 Corrosion

Corrosion is the destructive attack or deterioration of a metallic material due to chemical or electrochemical interaction with its environment [13], [14]. There are various ways of classifying corrosion. However, on the basis of the corrosion media, corrosion of metallic materials can be classified into three groups: wet corrosion, molten matter corrosion and dry corrosion [13], [15]. The most common type of corrosion occurring in water based electrolyte is the typical electrochemical process of wet corrosion. Corrosion can also occur in other fluids, e.g., fused salts or molten metals [1]. The addition of protective coating is the most effective way of preventing corrosion attacks on metallic substrates.

2.2.3 Corrosion of Coating-Substrate Systems

In a typical coating/metal substrate system, the metallic substrate has no direct contact with the corrosive environment. However, corrosion still takes place as a result of defects in the coating. In nitride based PVD coatings the corrosion protective properties depends on the surface defects. The corrosion properties of the coating are also dependent on the surface properties of the substrate as well as the chemical composition and microstructure. Particularly, defects such as pinholes that extend through the coatings have worse detrimental impacts. Defects can be present due to the inherent porosity of the coatings or macro defects that arise as a result of droplets on the surface of the coatings, also cracks on the coatings due to internal stress may cause defects [16]. These defects are considered the primary cause of failures in coating/metal systems.

Ş. Danişman and S. Savaş [16] reported that surface roughness of the substrate to be coated play a significant role on the corrosion behavior of the coating systems. They opined that substrate with high surface roughness results in non-uniform deposition of coatings. Consequently, there is poor film growth which leads to an increase in the possibility of presence of defects. Hence, multilayer coatings or coatings with higher thickness or smoother substrate surface will possess improved corrosion resistance [17].

The adhesion of coating to the surface of the substrate also plays a significant role in corrosion protection efficiency of the coating system. Proper adhesion is needed to ensure that coating do not delaminate, which may result to exposure of the substrate to corrosive media. The nature of coating and the cleanliness of substrate are the primary determinant of the adhesion properties of coatings [17].

Various studies have made comparisons of the corrosion and oxidation properties of different types of nitride based coatings (e.g. AlCrN, TiAlN and TiN). The studies of Vikas, *et al* [18], Zhang, *et al* [19] and Ding, *et al* [20] all noted the improved oxidation resistance and hardness of TiAlN over TiN coatings. It is general knowledge that coatings with titanium offers significantly improved hardness. However, titanium usually forms a porous and non-protective oxide scale in an oxidative or corrosive environment [18], [20]. This makes their corrosion and oxidative resistance inferior to CrN based coatings. The development of coatings void of titanium such as CrN based multicomponent nitrides (e.g. CrAlN and

AlCrN) have produced coatings with improved wear and corrosion resistance in comparison [20]. The improved oxidation and corrosion resistance have been attributed to the formation of protective oxide by the aluminum as well as the chromium which leads to suppression of the diffusion of oxygen [18], [20]. Xing, *et al* [20] have demonstrated that CrAlN coating exhibits higher corrosion resistance than TiAlN coatings in a sodium chloride solution. Similarly, [21] reported better cutting performance of CrAlN under high speed machining conditions.

2.2.4 Electrochemical Process of Corrosion

In most metals, corrosion occurs through electrochemical reactions at the interface between the metal and an electrolyte solution. Corrosion is an electrochemical reaction process, that is accompanying two simultaneously opposite reactions i.e., reduction and oxidation referred to as Redox reaction [1]and[22]. The rate of corrosion is determined by the equilibrium between this two opposing reactions [22].

In most electrochemical corrosion experiments, measurement of the open-circuit potential (OCP) is the first step. The open-circuit potential is the equilibrium potential that is assumed by a metal in the absence of electrical connections .In a polarization of an electrode from the OCP under steady-state conditions, the potential-current relationship is quantitatively described by the Butler-Volmer equation [19], [23], [24]. This equation takes both cathodic and anodic reactions on the same electrode into account, and is given as:

$$I = A \cdot i_0 \cdot \left\{ \exp \left[\frac{(1-\alpha)n \cdot F}{RT} \cdot (E - E_{eq}) \right] - \left[\exp - \frac{\alpha \cdot n \cdot F}{RT} \cdot (E - E_{eq}) \right] \right\} \quad (2.1)$$

where:

I : electrode current,

i_0 : exchange current density,

E : electrode potential,

E_{eq} : equilibrium potential,

A : electrode active surface area,

T : absolute temperature,

n : number of electrons involved in the electrode reaction

F : Faraday constant (9.65×10^4 C/mol)

R : universal gas constant

a : symmetry factor,

The corrosion current I_{corr} is essential in calculating the corrosion rates of metals, they are however very difficult to measure directly. The I_{corr} is the measured value of the anodic current or current at the anode at the E_{oc} (Open Circuit Potential). Despite the difficulty in direct measurement they can be estimated quantitatively by the use of various electrochemical techniques. The corrosion current and the corrosion rate of real systems are a function of different combinations of parameters such as the solution composition, nature of metal, temperature, movement of solution etc. [22].

Corrosions are mainly products of electrochemical reactions; hence corrosion processes are ideally studied by electrochemical techniques. In electrochemical studies, small surface area of the metal sample is used in modeling the metal in a corrosive environment. The metal sample is immersed in solution that simulates the corroding environment in which the metal will be exposed to. In this study approximately 1 cm^2 was an exposed surface area of the tested samples, while 3.5 wt. % NaCl solution is the corrosive medium. Additional electrodes were immersed in the solution, and all the electrodes were connected to a device called a potentiostat. A potentiostat allows to change the potential of the metal sample in a controlled manner and measure the current that flows as a function of applied potential [22].

In electrochemistry, the three electrode setup is the most widely employed electrochemical setup. The schematic of the 3 electrode setup is illustrated in Figure 2.1. It consists of the working electrode (WE), counter electrode (CE) and the Reference electrode (RE). The current will flow between the CE and the WE, and the potential difference is measured between the reference electrode and the sample [25].

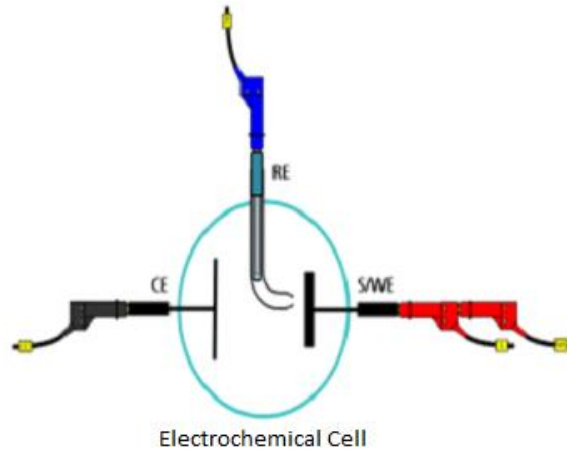


Figure 2.1: Schematic view of the 3 electrode setup[25].

Generally, an electrochemical reaction under kinetic control obeys the Tafel equation [22]. The Tafel plot is $\log I$ versus E . Mathematically, the Tafel equation is expressed as:

$$I = i_0 e^{\frac{2.303(E-E_0)}{\beta}} \quad (2.2)$$

where:

- I is corrosion current
- I_0 is a reaction-dependent constant called the exchange current;
- E is the electrode potential;
- E_0 is the equilibrium potential (constant for a given reaction);
- β is the reaction's Tafel constant (constant for a given reaction, with units of volts/decade)

In the Tafel equation only one isolated reaction's behavior is described. However, in real corrosion systems, there are two opposite reactions occurring simultaneously: the anodic and cathodic reaction. Figure 2.2 shows a typical Tafel plot, indicating the anodic and cathodic components of current.

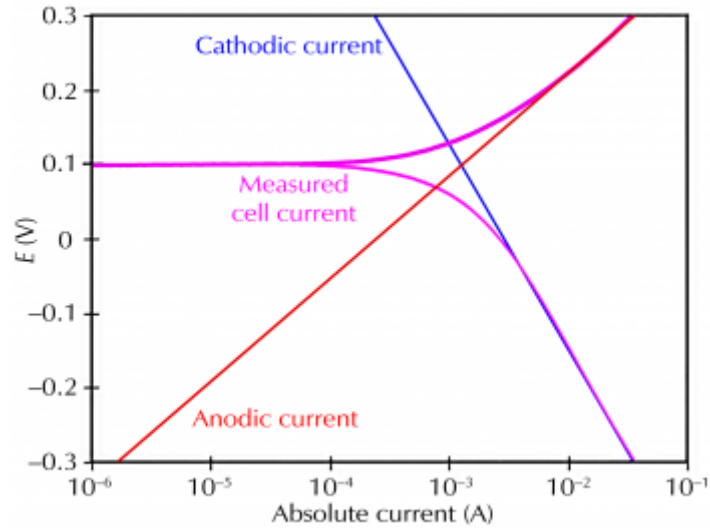


Figure 2.2: A typical Tafel plot [22].

The Butler-Volmer equation (Equation 2.2) can be obtained by the combination of the anodic and cathodic reactions.

$$I = I_{corr} e^{\frac{2.303(E-E_{corr})}{\beta_a}} - e^{\frac{2.303(E-E_{corr})}{\beta_c}} \quad (2.3)$$

where:

I is the measured current from the cell in amperes;

I_{corr} is the corrosion current in amperes;

E is the electrode potential

E_{corr} is the corrosion potential in volts

β_a is the anodic β Tafel constant in volts/decade;

β_c is the cathodic β Tafel constant in volts/decade.

To extrapolate the Tafel anodic and cathodic linear regions in a polarization curve, an intersection of curves can be used to obtain both E_{corr} and i_{corr} . Tafel constants (in unit of

V/decade) obtained from both the anodic and cathodic portions of the Tafel plot are shown in Figure 2.3.

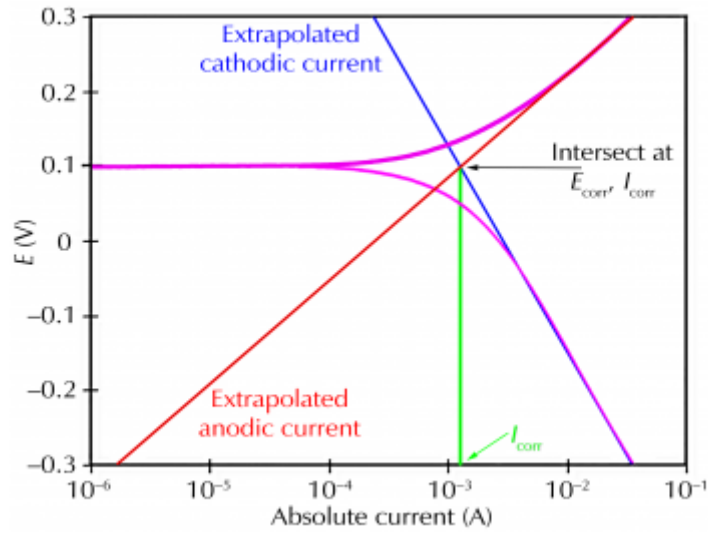


Figure 2.3: Classic Tafel analysis [22]

The Butler-Volmer equation (Equation 2.1) can be converted to the Stern-Geary relation (Equation 2.6) under this condition [26]: the potential is restricted to be very near to E_{corr} . The approximation of the exponential terms of the Butler-Volmer equation with the first two terms of a power-series expansion and simplification will obtain a form of the Stern-Geary equation [22]:

$$i_{corr} = \frac{\beta_a \beta_c}{2.303 R_p (\beta_a + \beta_c)} \quad (2.4)$$

where:

i_{corr} : the corrosion current (Amps)

β_a the anodic Tafel slope constant (Volts per decade)

β_c the cathodic Tafel slope constant (Volts per decade)

R_p the polarization resistance value determined from the linear polarization experiment.

2.3 Surface defects in PVD Hard Coating

Growth defect is a common phenomenon in all coating technologies [4], [27]–[29]. Although, hard coatings possess inherently good corrosion resistance, the coatings system (substrate-coating) usually suffer from adverse corrosion as a result of the presence of defects [30]. Any imperfection formed on substrate surface during pre-treatment or growth defects in hard coatings prepared by physical vapour deposition are very often drawbacks in their applications [27]. These defects in form of craters and pin holes in the coating compromises the performance of the coating.

On sites where defects extend through the coating, pitting corrosion can easily take place; this is recognized as one of the leading drawbacks of hard coatings. Typically, macro- and micro defects in hard coatings occur during deposition [27]. According to Gselman *et al.*, [31] and M. Panjan *et al.*, [29] any defects smaller than 1 μm are categorized as microdefects. On the other hand macro defects are in forms of large and shallow craters and nodular defects, usually with a diameter of greater than 5 μm [31].

2.3.1 Surface Defect Formation in Hard Coatings

2.3.1.1 Mechanical Pre-Treatment of Substrate

Some defects are already present during the mechanical pre-treatment of the substrate. During grinding and polishing, the matrix of the substrate is removed faster. If the pressure during polishing is too high and polishing time too large, then the inclusions could be torn out of material and a pit with dimensions of inclusion is left behind [27].

2.3.1.2 Cleaning Procedure

The cleaning procedures are also an important origin of defects in a coating system. Cekada *et al.*, [27] suggested demagnetizing the substrate prior to cleaning; this is to avoid problems in removal of debris and polishing residue from the surface. Ultrasonic cleaning in an alkaline agent is necessary to reduce the surface contamination to the barest minimum. After rinsing in de-ionized water, the substrates must be dried in hot air as quickly as possible while the residual water film will stick dust particles to the surface. Fine air and water filters

must be used in order to minimize the concentration of particles in de-ionized water and dry air.

Dust particulates that fall on substrate during batching or during pumping of the vacuum chamber can also be responsible for the inclusion of defects on the surface of the substrate. It is recommended that a special component which reduces turbulent airflow to minimum during rough pumping (up to 100mbar) be incorporated into the system.

2.3.1.3 Deposition Processes

Most hard coating defects arise during the process of deposition [27]. The defects normally originates from microparticles that flake during heating and deposition from coated components of vacuum system and incorporate in the growing coating [27], [30], [32]. Theses defects can be avoided by removing dust before each batch; also the fixtures and other components have to be cleaned by blasting. This is advisable only if the thickness of the deposited coating is more than few microns. However, these procedures still does not completely eliminate the presence of defects. The second common origin of defects is arcs during etching and deposition steps. They can cause the emission of microparticles that incorporate in coating during its growth. All impurities on targets and substrates increase the arc tendency.

2.3.2 Characterization of Surface Defects

Surface defects of coatings can be visualized with the aid of an optical microscope but the lateral and depth resolution is not sufficiently good [27], [29]. There is also a possibility of employing the optical profilometer in the characterization of surface defects. However, in spite of the high vertical resolution (approximately 3 nm) of the profilometer, it is highly difficult to distinguish individual shallow defects among many peaks in the profile. This is especially true when the aspect ratio (height-to-width) of such peaks is too small.

The scanning electron microscope (SEM) is able to distinguish high lateral and also has a better depth resolution. The morphology of the surface of hard coatings consists of the submicro-, micro- and macrodefects, which are non-uniformly distributed [27]–[29]. The AFM (Atomic Force Microscopy) as compared to the SEM gives some additional data (lateral resolution down to atomic scale, surface roughness S_a , 3D image), but its use is

limited due to relatively small scanning area [27]–[29]. The surface morphology can be a consequence of preferential sputtering during ion etching. In literature, there seems to be no conventional method of naming observed defects in coatings. They are mainly descriptive, for example *cone-like defects*, which describes the shape of the microparticles inclusions on the surface of the coatings Figure 2.4(1). Another example is the defect described in Figure 2.4 inset 2 is referred to as *crater like defects* by [27], meanwhile the same form of defect is described as *open void/through voids defects* in [33] (Figure 2.5c). Both defects are the same in nature and are both caused by high compressive stress in coatings, above a critical thickness. Yet they are named differently, this buttresses the lack of conventional nomenclature of observed coating defects. This disparity is common in literature, only the *cone-like defects* and *pin-hole defects* are universally named similarly.

Cekada et al., [27] reported four types of defects as observed on planar SEM micrograph of CrN and TiAlN hard coatings. They are majorly classified into four namely: big, shallow craters (diameters of 5-40mm), cone structure defects with diameter from 1 to several mm, and dish like holes arising from wrenching of the cone structure. The morphology of the defects is indicated in the insets in Figure 2.4: insets 2 and 4 represents shallow craters of few microns in diameter, while inset 3 indicates a cone structure defect. The study explained that the cone structure defects are a result of poor adhesion of the coating matrix to the substrate. High level of residual stress due to the thickness (i.e. when above critical thickness) of hard coating is responsible for the observed decohesion and delamination of coating [27]. Also, the crater like defects is due to rough and porous microstructure.

Similarly, Panjan, *et al* [33] studied growth defects in PVD hard coatings. The defects are described as, nodular or flake defects resulting from debris and foreign particles from the vacuum chambers that attach to the substrate before deposition Figure 2.5a (and Figure 2.4 inset 3), Open void defects (Figure 2.5c), similar to the crater like defects observed by [27] (Figure 2.4 inset 2 and 4), Cone like defects and pin-hole defects and defects in the form of micro droplets.

Both [27] and [33] noted that defects in the form of micro droplets are a result of arcing, they result from impurities on the targets and substrate which increases the arc tendency during deposition. This will consequently lead to micro droplet emission during film growth. Similarly, the literature reviewed agreed that the pin-hole defects poses the most detrimental threat to the coating systems' corrosion resistance, in that they allow the substrate to be

exposed to the corrosive media. This is because the pin-holes extend through the coating thereby giving corrosive media access to the substrate [27], [31], [34], [35].

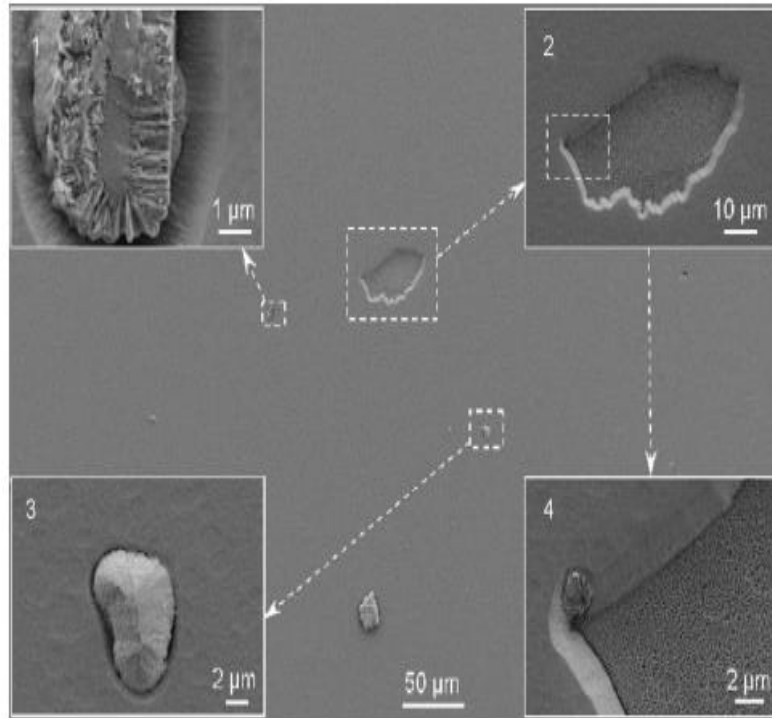


Figure 2.4: Planar SEM micrographs of CrN hard coating showing the morphology of typical defects [23].

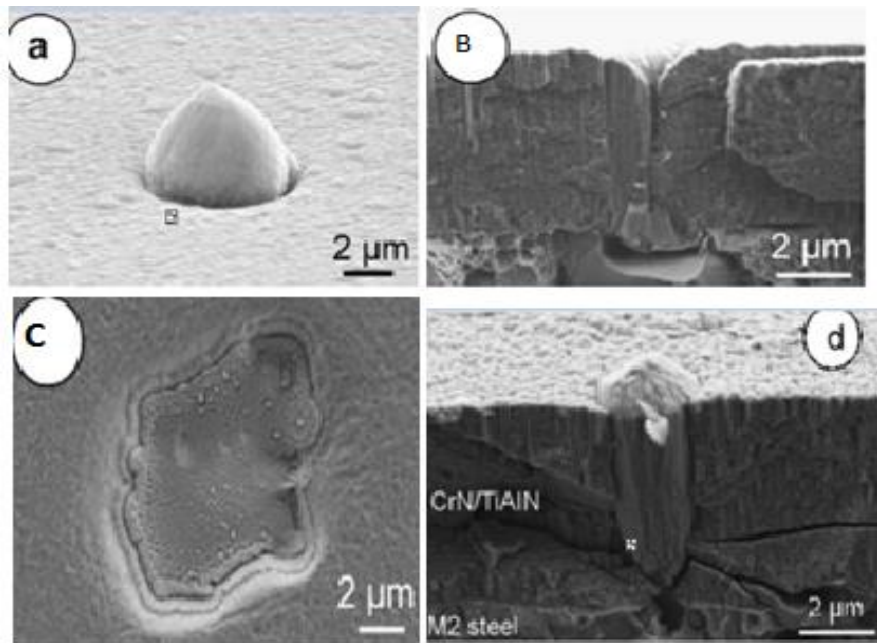


Figure 2.5: Defect Morphologies: a cone-like inclusions on surface of ASP 310 tool steel [36] (b) cross- section SEM of pinhole defect [36] (c) through voids or dish like craters [36] (d) spherical pin-hole defect, which extends through the whole coating [30].

The origin of most of these defects is inhomogeneous coating growth caused by microparticles (which flake during heating, etching and deposition from the shields, rods, fixtures and dust from pre-treatment) [27], [30]. Growth defects can be minimized by ensuring proper cleaning of substrate before deposition.

2.4 Coating Deposition Technologies

Deposition of coatings on a substrate can be achieved by vapor deposition processes. This processes helps in achieving the desired degree of accuracy in terms of ensuring uniformity of coating materials over the substrate and coating thickness. Figure 2.6 summarizes the different coating deposition processes typically in use.

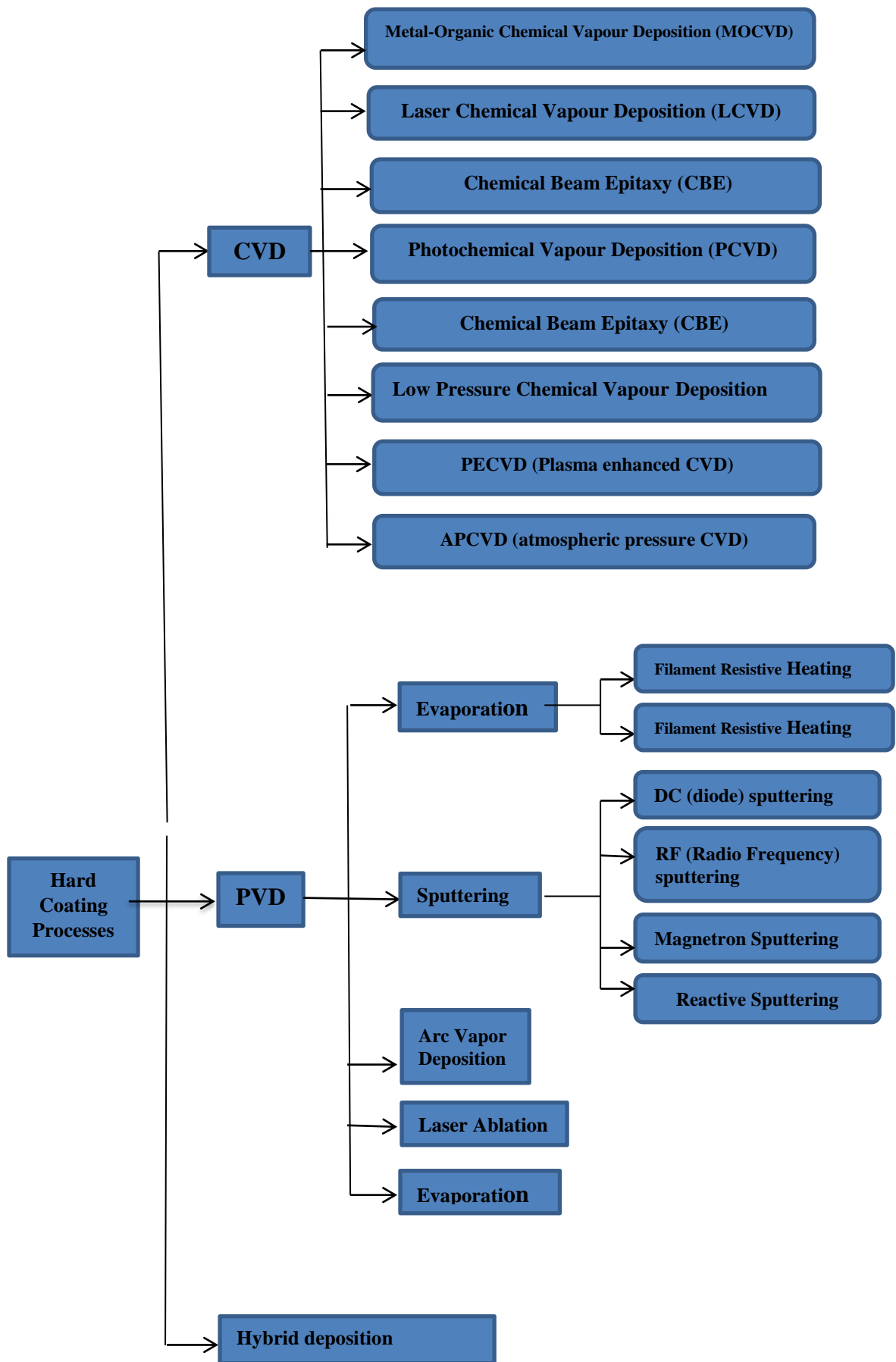


Figure 2.6: Deposition processes of thin hard coatings [36].

2.4.1 CVD (Chemical Vapour Deposition)

Generally, CVD involves the deposition of a solid on a heated surface from a chemical reaction in the vapor phase. The deposition involves homogeneous gas phase reactions, which occur in the gas phase. The substrate surface is exposed to the volatile coating precursors which then reacts and decomposes on its surface to generate the desired coating. The CVD process is well adapted to the deposition of multi-layered coatings because the process is relatively easy to regulate using various gases [36]. CVD coatings are characterized by finer grained microstructure, improved porosity and generally improved purity.

There are various forms of the CVD processes namely [37]:

- Atmospheric Pressure Chemical Vapour Deposition (APCVD)
- Low Pressure Chemical Vapour Deposition (LPCVD)
- Metal-Organic Chemical Vapour Deposition (MOCVD)
- Plasma Assisted Chemical Vapour Deposition (PACVD) or Plasma Enhanced Chemical Vapour Deposition (PECVD)
- Laser Chemical Vapour Deposition (LCVD)
- Photochemical Vapour Deposition (PCVD)
- Chemical Vapour Infiltration (CVI)
- Chemical Beam Epitaxy (CBE)

2.4.2 PVD (Physical Vapour Deposition)

The development of PVD coatings in the 1980s has boosted the application of coatings in various areas of applications, such high speed tooling and corrosion resistance applications. In PVD coatings there is a deposition of thin films (2-10 microns) on the surface of components. There are three distinct stages involved in PVD coating deposition, namely evaporation: which involves the removal of material from the target or source (cathode), Transportation, which involves the movement of the evaporated material from the source to the substrate. Then there is condensation, which involves the nucleation and growth of the coating on the surface of the substrate.

Physical vapor deposition makes use of variations of vacuum deposition techniques for depositing thin films by condensation of vaporized form of the desired material. The coating material for deposition is usually removed by arc-discharge or sputtering. The material of the

coating is transported through a plasma medium, which is a collection of charges. The constituents of the particles can be influenced by a magnetic field which makes travel in straight line to the surface of the substrate. Depending on the employed techniques in generating the plasma, different characteristics can be incorporated into it. A PVD coating is formed when plasma constituents and reactive gases combine on the substrate surface. Also, on energy; the degree of ionization of the metal ions; and mobility of the atoms condensing on the substrate surface directly affects the properties of the coating.

Various PVD technologies exist, which includes arc deposition, magnetron sputtering, laser ablation and evaporation. These methods have also been incorporated with technological enhancement that yield high deposition films with high adhesion and varying microstructure. Various forms of the magnetron sputtering and arc deposition are the most widely employed PVD deposition technology.

Figure 2.7 illustrates a schematic of the PVD process based on magnetron sputtering. This process involves the gradual removal of the coating material from the metal target by bombardment with argon ions. In this process plasma is created and positively charged ions from the plasma are accelerated by an electrical field superimposed on the negatively charged electrode (the target). The ejected atom will move in a typical line-of-sight cosine distribution from the face of the target. These atoms will be ejected in a typical and will then condense on the surface of the intended substrate which is already placed closely to the cathode of the magnetron sputtering. In magnetron sputtering deposition, a closed magnetic field is utilized in trapping electrons, these results in improvement of efficiency of the initial ionization process. It also allows generation of plasma at lower pressures. During the coating process the substrates are rotated to ensure uniform coating thickness everywhere.

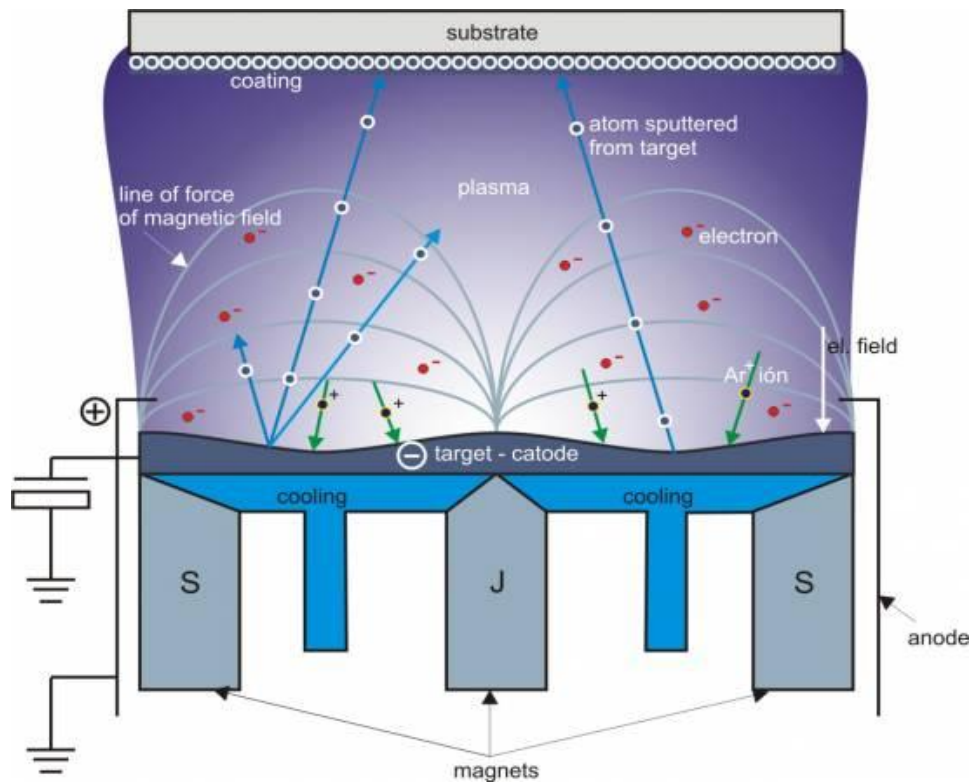


Figure 2.7: Schematic of the PVD process based on magnetron sputtering [38].

The major advantages of PVD coating process are that: they impart improved hardness and wear resistance, reduced friction and improved oxidation in comparison with CVD. Also, in contrast to CVD process, PVD process generally induces desirable compressive residual stresses in the coating which is important for intermittent cutting processes like ball end milling. In addition, PVD processes can generate very thin coatings which are able to retain a very sharp cutting edge. Overall PVD processes are more flexible and have a wider range of applications than CVD coatings [36].

2.4.3 TiAlN, AlCrN and TiCN coatings.

Most metal nitrides have exhibited superior characteristics such as high hardness, wear resistance, corrosion and oxidation resistance, chemical stability and low friction coefficient. These properties have ensured the wide range of application in which they are employed [39], [40].

Chim *et al* [41] in their studies deposited TiN, CrN, TiAlN and CrAlN (with Al/Ti or Al/Cr atomic ratio around 1:1) on stainless steel substrates by a lateral rotating cathode arc

technique. They have investigated the influence of oxidation behavior on overall hardness of the four PVD coatings (TiN, CrN, TiAlN and CrAlN). The results of the research can be summarized thus: TiAlN and CrAlN coatings showed better oxidation and corrosion resistance as compared to TiN and CrN. Of particular interest is the TiN coating which was evidently oxidized and became soft at 500 °C, and completely delaminated from the substrate at 800 °C. This highlights the limitation of TiN coating, especially in high temperature machining. TiAlN coating started to oxidize at 600 °C and its hardness decreased significantly at 700 °C. CrAlN showed the best oxidation resistance of all the studied coatings.

Panjan, *et al* [34] and [30] in their studies investigated the relationship of deposition parameters e.g. deposition pressure, substrate bias, and deposition temperature, on the structure and electrical resistivity of TiN. The conclusion was that: the electrical resistance was significantly affected by the amount of nitrogen present, phase structure, and defect density. It was also reported that grain size played a minor role in the electrical resistivity of TiN films. A significant decrease in the defect density was associated with an increase in the deposition temperature. Also, increase in the grain size of TiN films is related to a linear decrease in the electrical resistivity of TiN films.

It is generally expected that in most acidic and alkaline solutions thick TiN coatings would possess good corrosion resistance. It is however reported that a thin TiN coating can be severely affected by a corrosive medium [17]. A coating of less than 6 μm will result in pitting corrosion [17]. Coating with such thickness is not always feasible during depositions. This limitation of TiN coating has led to the development of more recent TiAlN coatings. They have attracted enormous attention due to the improved properties they possess.

It has been reported that the alloying of PVD transition metal nitride, for example the alloying of TiN matrix with aluminum results in the control of size and density of micropores [17]. This has resulted in the development of Ternary coatings such as AlCrN, TiCN, and TiAlN. Compared to TiN, the ternary coating system (Ti, Al)N shows an increasing hardness even at elevated temperatures. In dry drilling tests, an improved wear behavior was found compared to TiN, which was due to the superior high temperature properties of (Ti,Al)N films [18], [20], [42]. It has also been reported that the properties of TiAlN increases with aluminum content. However, in the studies of V.K Grips *et al* [2] it

was noted TiAlN coatings with 50 % concentration showed the highest corrosion resistance. Furthermore, it was indicated that further increase in Al concentration results in reduction of adhesion of the TiAlN coating on the substrate.

The performance of PVD (Ti,Al)N as a commercial coating on cutting tools was reported in the study of Leyendecker *et al.*[43], superior wear resistance in the machining of cast iron was reported. They observed that the performance of (Ti, Al)N coated tools were superior to both TiN and TiN-WC/C coated tools.

The comparison of tribological behaviors of AlCrN and TiAlN coatings—applied by physical vapor deposition by J.Mo, *et al* [44] indicated that AlCrN shows better wear resistance, anti-oxidation and anti-spalling characteristics.. The study concluded that AlCrN will probably have a wider range of tribological applications than the TiAlN coating under the condition of sliding wear.

Many studies have indicated the excellent characteristics of TiCN coatings. Many of the studies of TiCN coatings have been centered on its uses in biomaterials. The studies of Hollstein and Louda [45] evaluated the corrosion resistance of TiCN-coated stainless steel as a PVD protective layer on surgical instruments. The results pointed to a slow kinetics of the corrosion processes and a good biocompatibility of the PVD film. Similarly, the study of [46] and [47] compared the tribological properties of TiCN and some other coatings, it was found out that TiCN coatings had superior tribological properties compared to TiN. However, in most studies they have shown inferior tribological properties as compared to AlCrN and TiAlN. On the other hand they have shown the best biocompatibility, hence their wide use in biomedical applications [48]-[49].

3 Materials and Experimental Procedures

3.1 Substrate Deposition and Preparation

3.1.1 Coating deposition

Deposition of hard coating can be carried out by different physical and/or chemical deposition processes, which includes thermal spray, magnetron sputtering, plasma-enhanced CD, ion implantation and cathodic arc deposition (CAD)[50]. Of all the processes, CAD is the one of the most suitable technologies due to its characteristics, such as nearly fully ionized plasma and high energy ions [20]. CAD systems can deposit hard coatings with high density and strong adhesion. However, the conventional planar arc systems usually deposit hard coatings with macro defects, including both inclusions and voids, due to the incorporation of the micro-metal droplets emitted from the cathodes, which also reduce the corrosion resistance of hard coatings [51]. A recent new cathode arc technology based on rotating cathodes was developed, and it has been included into advanced coating system π^{80} developed by *PLATIT* [52].

For this work the AlCrN, TiAlN, and TiCN coatings were all deposited on the AISI 316 steel substrate by a Platit π^{80} system (Figure 3.1) under a reactive nitrogen atmosphere using Lateral Rotating ARC-Cathodes (LARC) technology. Substrate specimens were cleaned in ultrasonic bath with isopropanol before deposition. Immediately after the cleaning procedure, samples were placed into the vacuum chamber and sputter-cleaned in argon plasma with a bias voltage of -850V at 425 °C for 1 hour. This helps to reduce contaminants and oxide on the surfaces of the samples. The deposition temperature was 450 °C for each coating.



Figure 3.1: The Platit π 80 deposition system.

3.2 Evaluation of Coating

3.2.1 Measurement of coating thickness

Coating thickness has been evaluated by analysis of the cross-section micrographs of the samples. Also, the measurements were confirmed using the kalotest method with the kaloMAX tester. Surface roughness was measured with Perthometer Concept PGK 120 by Mahr and nanohardness was received from *PLATIT π80* system.

3.2.2 Compositional and Microstructural characterization

3.2.2.1 Scanning Electron Microscope (SEM) analysis

Scanning electron microscopy (SEM Hitachi TM-1000 Tabletop) was used to determine surface topography and microstructure of the coatings and AISI 316 steel substrate. The

surface topography was examined by SEM under secondary electron (SE). Deposition defects such as embedded nodule, void, pinholes, inclusions etc. were observed from the SEM images.

3.2.2.2 Energy Dispersive Spectroscopy analysis

Compositional analysis of the samples were also conducted using the EDS software on the SEM Hitachi TM-1000 Tabletop



Figure 3.2: The SEM Hitachi TM-1000 Tabletop.

3.3 Electrochemical Characterization of corrosion behavior of coatings

The corrosion characteristics of the AlCrN, TiCN, TiAlN-coated AISI 316L steel and uncoated substrate was investigated using the potentiodynamic polarization in 3.5% NaCl solution at room temperature ($23^{\circ}\text{C} \pm 2^{\circ}\text{C}$). The measurements were performed by an Autolab PGSTAT30 galvanostat/potentiostat system. The selected system consists of a three-electrode electrochemical cell with platinum sheet as and a calomel (Hg/HgCl in saturated KCl) electrode as the RE. Specimens served as the working electrodes. The sample for measurements were carefully covered in hot melted silicone glue (non-conductive), the exposed surface area to the corrosive medium was approximately 0.9 cm^2 . Samples were cleaned with acetone and distilled water before conducting every test. The sample was positioned in such a way that the Luggi capillary of the reference electrode was closer to the WE than to CE.

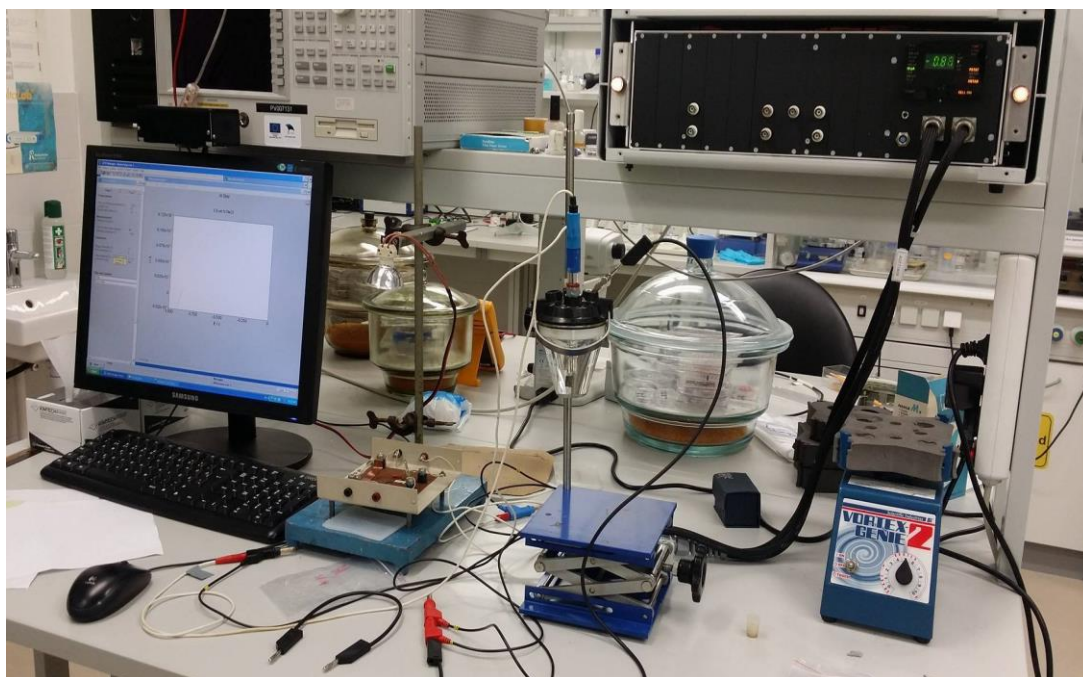


Figure 3.3a: The Autolab PGSTAT30 galvanostat/potentiostat system.

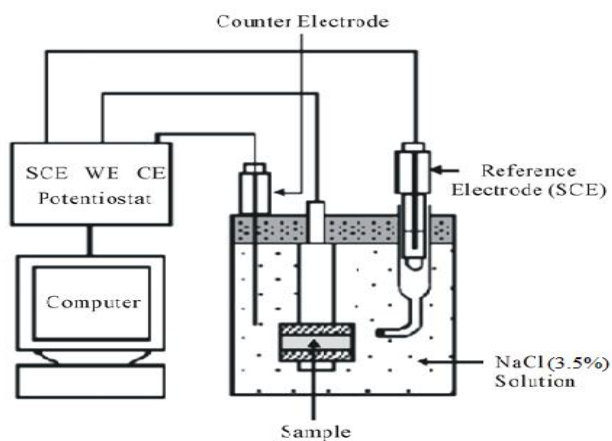


Figure 3.3b: A schematic representation of the of the three-electrode electrochemical cell used. WE (Working Electrode), CE (Counter Electrode (Platinum sheet), RE (Reference electrode (Hg/HgCl in saturated KCl solution)).

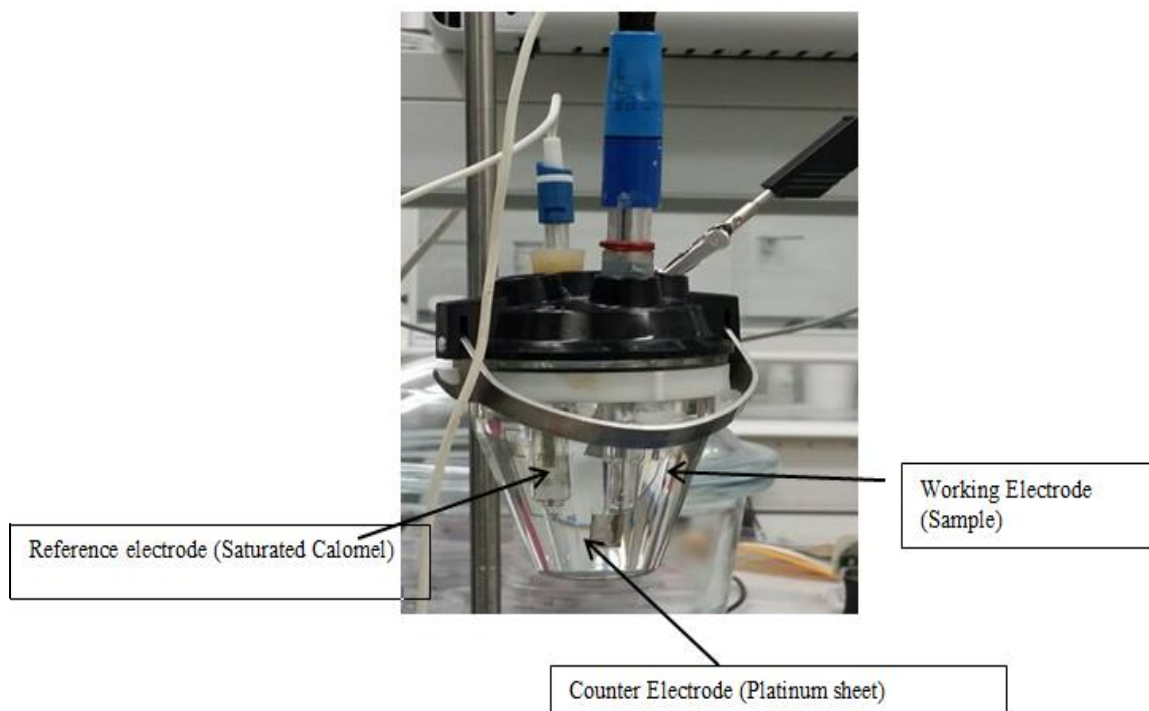


Figure 3.3c: The three-electrode electrochemical cell system used.

3.3.1 Operational Procedures

3.3.1.1 Open Circuit Potential

The open OCP also known as the corrosion potential is a summation of the half-cell reaction potentials in an electrolyte. It is monitored by measuring the potential against a reference electrode using a high impedance voltammetry or electrometer in such a way that no current flows between the electrodes in question and the reference electrode. The potential vs. time response data was collected and stopped when the specimen had reached a steady-state potential with the 3.5% NaCl. The corrosion potential is the basis for the linear and potentiodynamic polarization experiments. The ASTM G-69 standard practice for testing OCP was followed.

3.3.1.2 Polarization and Potentiodynamic Polarization Test

Principles of Measurement

When a metal/alloy electrode is immersed in an electrolytically conducting liquid of sufficient oxidizing power, it will corrode by an electrochemical mechanism. This process involves two, simultaneous, complementary reactions. At anodic sites, metal will pass from the solid surface into the adjacent solution and, in so doing, leave a surplus of electrons at the metal surface. The excess electrons will flow to nearby sites, designated cathodic sites, at which they will be consumed by oxidizing species from the corrosive liquid [53].

The polarization resistance test is a non-destructive electrochemical technique in which the potential of a metal is scanned over a small range relative to the open circuit potential and the resulting current is measured. In this method, a small potential scan, ΔE (t), defined with respect to the corrosion potential ($\Delta E = E - E_{corr}$) is applied to the metal sample. The resultant current is recorded. The material is polarized, typically on the order of ± 10 mV, relative to its Open Circuit (OC) potential.

As the potential of the working electrode (the tested specimen) is changed, a current will be induced to flow between the working and counter electrodes, and the material's resistance to polarization can be found by taking the slope of the potential versus current curve. Using the slope of the linear portion of the data, the polarization resistance value, R_p , can be obtained. This resistance can then be used to find the corrosion rate of the material using the Stern-Geary equation [26].

$$i_{corr} = \frac{\beta_a \beta_c}{2.303 R_p (\beta_a + \beta_c)} \quad \text{Equation (3.1)}$$

where:

i_{corr} : The corrosion current (Amps)

β_a The anodic Tafel slope constant (Volts per decade)

β_c The cathodic Tafel slope constant (Volts per decade)

R_p The polarization resistance value determined from the linear polarization experiment.

Polarization resistance (R_p) can be obtained from the following relationship:

$$R_p = (\Delta E / \Delta i)|_{\Delta E \rightarrow 0} \quad (3.2)$$

where:

ΔE Polarization potential (V);

Δi Polarization current (Amp).

The polarization resistance increases with a decrease in corrosion current.

Stern-Geary constant calculation from known Tafel slopes in cases where one of the reactions is purely diffusing controlled is given by:

$$B = \frac{\beta}{2.303} \quad 3.3$$

where:

β The activations controlled Tafel slope in V.decade⁻¹;

B Stern-Geary constant, V;

Tafel slope estimation from the rate controlling step in the mechanism of reaction in case where reaction mechanism is known in detail:

$$\beta = \frac{K.R.T}{n.F} \quad 3.4$$

where:

K a constant (for simple one electron reactions, K is usually found to be 2)

R the perfect (molar, ideal, universal) gas constant, 8.314 J.mol⁻¹.K⁻¹

T the absolute temperature, K

n the number of electrons involved in the reaction step;

F Faraday's constant, 6.202.10²³.mol⁻¹

At 25⁰C (298.15K), $\left(\frac{R.T}{2.303.F}\right)$ is 59.2mV.decade⁻¹

Corrosion current density calculation from the polarization resistance and Stern-Geary constant:

$$i_{corr} = \frac{B}{R_p} \quad 3.5$$

where:

- i_{corr} corrosion density $\mu\text{A}/\text{cm}^2$;
 B Stern-Geary constant, V;
 R_p the true polarization resistance Ωcm^2 .

The effect of solution resistance is a function of cell geometry, but the magnitude can be estimated by the following expression:

$$R_p = R_a - \rho_{el} \cdot l \quad 3.6$$

where:

- R_a the apparent polarization resistance, Ωcm^2 ;
 ρ_{el} the electrolyte resistivity in Ωcm ;
 l the distance between the specimen and the Luggin capillary (also Luggin probe, Luggin tip, or Luggin-Haber capillary) of reference electrode, cm;
 R_p the true polarization resistance Ωcm^2 .

Potentiodynamic techniques introduce an additional error from the capacitive charging effects. In this case the magnitude of the error is proportional to scan rate:

$$I_{total} = I_f + c \left(\frac{dV}{dt} \right) \quad 3.7$$

where:

- I_{total} the cell current
- I_f the Faradaic current associated with anodic and cathodic processes;
- C the electrode capacitance;
- $\left(\frac{dV}{dt} \right)$ the scan rate

The capacitance charging effect will cause the calculated polarization resistance to be in error. Generally this error is small with modest scan rates.

The corrosion current density can be used to evaluate the corrosion rate of the metal/coating using Equation (2)

$$CR = \frac{i_{corr} * k * EW}{D * A} \quad \text{Equation (3.8)}$$

where:

- CR: The corrosion rate in millimeters per year (mpy)
- i_{corr} : The corrosion current in amps
- k: A constant, 1.288x10⁵ millimeters (amp-mm-year)
- EW: The equivalent weight in grams per equivalent
- D: The density of the sample in grams per cubic centimeter
- A: The sample area in square centimeters

3.3.1.3 Potentiodynamic Testing

The potentiodynamic polarization measurements were conducted after a steady-state E_{oc} test and were carried out with a scanning range from an initial potential of -0.633 V vs. the E_{oc} to a final potential of +1200 mV. The scan rate was 5 mV/s. The corrosion potential (E_{corr}), corrosion current density (i_{corr}) and corrosion rate were evaluated from the Potentiodynamic polarization. The Tafel plot was obtained after the electrochemical measurements. The corrosion potential and corrosion current density were obtained from the Tafel plot. The

corrosion current is obtained using the Stern–Geary equation [26] . The ASTM G-5 and G-59 standard practices for making potentiodynamic polarization measurements were followed throughout these experiments.

3.3.1.4 Protective Efficiency Calculation

The protective efficiency was calculated from the polarization test results. The protective efficiency P_i (%) of the films can be evaluated quantitatively according to Equation 3.9 [3], [48], [54].

$$P_i(\%) = \left[1 - \left(\frac{i_{corr}}{i_{corr}^0} \right) \right] \times 100 \quad 3.9$$

where:

i_{corr} and i_{corr}^0 indicates the corrosion current density of the film and substrate respectively.

3.3.1.5 Porosity Determination

The porosity of the coating is an important parameter for evaluating the defect densities [19]. A low porosity indicates a favorable protective efficiency. The higher the porosity of the coating the higher is its tendency to allow significant galvanic corrosion to occur between the substrate and the coating [55], [56]. In evaluating the porosity of protective coatings various electrochemical techniques can be adopted. In the cases of electrochemically noble or electrochemically stable coatings, a simple polarization resistance method is well suited [3], [48], [57]. On the assumption that the coating is electrochemically inert at low anodic overpotential, the porosity of the coating can be estimated using the relation in Equation 3.4 [3], [48], [58].

$$P = \left(\frac{R_{ps}}{R_p} \right) \times 10^{-\left(\frac{\Delta E_{corr}}{\beta_a} \right)} \quad 3.10$$

where:

P the total coating porosity;
 R_{ps} and R_p the polarization resistance of the substrate and the coating, respectively;

β_a the anodic Tafel slope of the substrate and
 ΔE_{corr} the difference between the corrosion potentials of the coating and the substrate.

Calculation of the corrosion rate according to Faraday's law

Penetration rate:

$$CR = K_1 \cdot \frac{i_{corr}}{\rho} \cdot EW_{alloy} \quad 3.11$$

where:

CR - penetration rate (the thickness loss per unit time) mm.year⁻¹;
 K_1 - 3.27x10⁻³ mm.year⁻¹ (only consistent valence groupings were used);
 i_{corr} corrosion Density $\mu\text{A}/\text{cm}^2$;
 ρ alloy density g. cm³
 EW_{alloy} the alloy equivalent weight (dimensionless)

The alloy equivalent weight EW_{alloy} can be calculated thus:

Equivalent weight:

$$EW = \frac{W}{n} \quad 3.12$$

where:

EW Equivalent weight;
W exposed specimen area;
n the number of electrons required to oxide an atom of the element in the corrosion process (the valence of element)

Alloy Equivalent weight:

$$Q = \sum \frac{ni f_i}{w_i} \quad 3.13$$

- Q the electron equivalent for 1g of an alloy;
 f_i the mass fraction of the i^{th} element in the alloy;
 w_i the atomic weight of the i^{th} element in the alloy;
 N_i the valence of the i^{th} element in the alloy;

Mass loss rate:

$$MR = K_2 \cdot i_{corr} \cdot EW_{alloy} \quad 3.14$$

where:

- MR mass loss rate, ($\text{g} \cdot \text{m}^{-2} \cdot \text{day}^{-1}$);
 K_2 $8.954 \times 10^{-3} \text{ g} \cdot \text{cm}^2 \cdot \mu\text{A}^{-1} \cdot \text{day}^{-1}$
 i_{corr} corrosion Density $\mu\text{A}/\text{cm}^2$;
 EW_{alloy} the alloy equivalent weight (dimensionless)

4 Results and Discussions

4.1 Surface Morphology

4.1.1 Coating thickness

The coating thickness of the coatings is presented in Table 4.1

Table 4.1: Coating thickness

Samples	Thickness of coating (μm)
TiCN	3.7
TiAlN I	1.5
AlCrN	3.6
TiAlN II	2.4

4.1.2 Defects on coatings

The various examples of defects that are associated with the coatings have been characterized with SEM. The observed defects are outlined in Figures 4.1- 4.6. The commonly occurring surface defects in PVD coatings as discussed in chapter 2 have been identified, notably macroparticles, open voids (craters) and pinholes. Macroparticles are formed as a result of unreacted metallic droplets been ejected on the substrate from the source during evaporation. There is an acceleration of these particles towards the substrate at very high speeds; they are consequently embedded on the surface of the coating films. Macroparticles on the surface of the coating affects the tribological properties by acting as a third-body abrasives, therefore it speeds up the rate of coating wear [59], they generally have more detrimental impact on the coating performance; especially its protective efficiency. Examples of macroparticles defects are indicated Figure 4.1 which is similar to the defect observed by SEM in [27] and [33].

The mechanism of film growth associated with PVD coatings gives rise to pinhole defects, which are almost unavoidable. Generally, pinholes protrude through the film, which leads to

an exposure of the substrate which it is intended to protect. This consequently compromises the corrosion resistance of the coatings, it is therefore imperative to minimize these defects. Figure 4.4 presents an example of pinhole defect, although it cannot be concluded that it protrudes through the coating. Further characterization techniques such as AFM (Atomic Force Microscopy), FIB (Focus Ion Beam) and 3D profilometer are essential to arrive at a more definitive conclusion. In Figure 4.5 a larger defects is indicated. The larger defects may have the same detrimental impact on the coatings as the pinholes if they also protrude through to the substrate. Figure 4.2 indicates a nodular crater like defects similar to that observed on the CrN coatings by Cekeda, *et al* [27] and Panjan, *et al* [33].

Defects in the form of cracks generally occur in area of coating with increased thickness. A network of interconnected cracks on the surface TiAlN coating is presented in Figure 4.3. They result from contamination on the surface of the coating before deposition. Large internal stresses are also a major factor resulting in cracks in coatings. The TiAlN II which shows less defect concentration is shown to possess better corrosion resistance and much lower porosity as compared to the TiAlN sample with network of interconnected cracks.

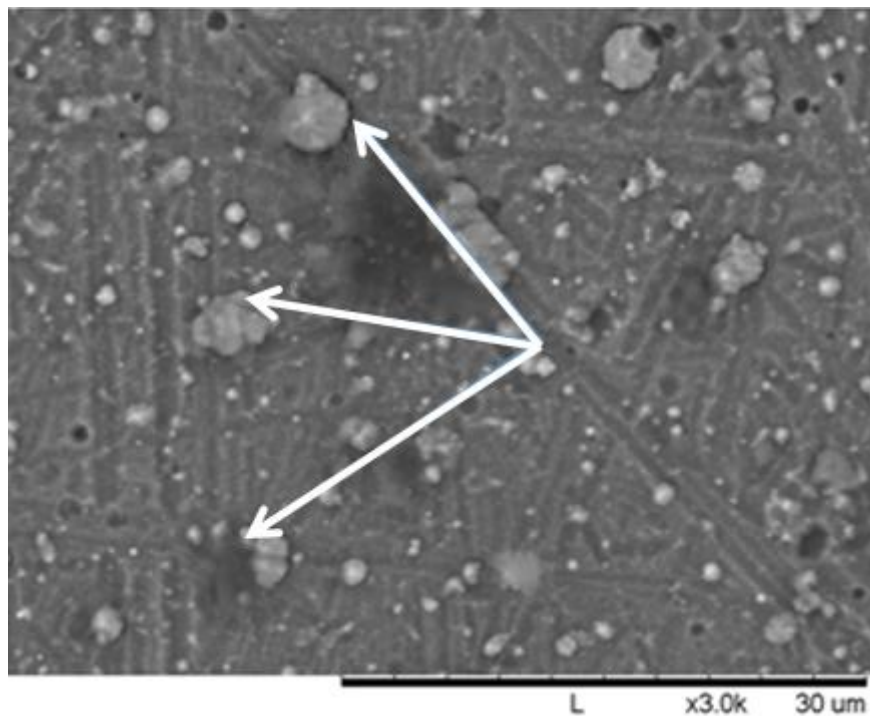


Figure 4.1: SEM micrograph showing: Sphere-like macrodroplets on the AlCrN coating.

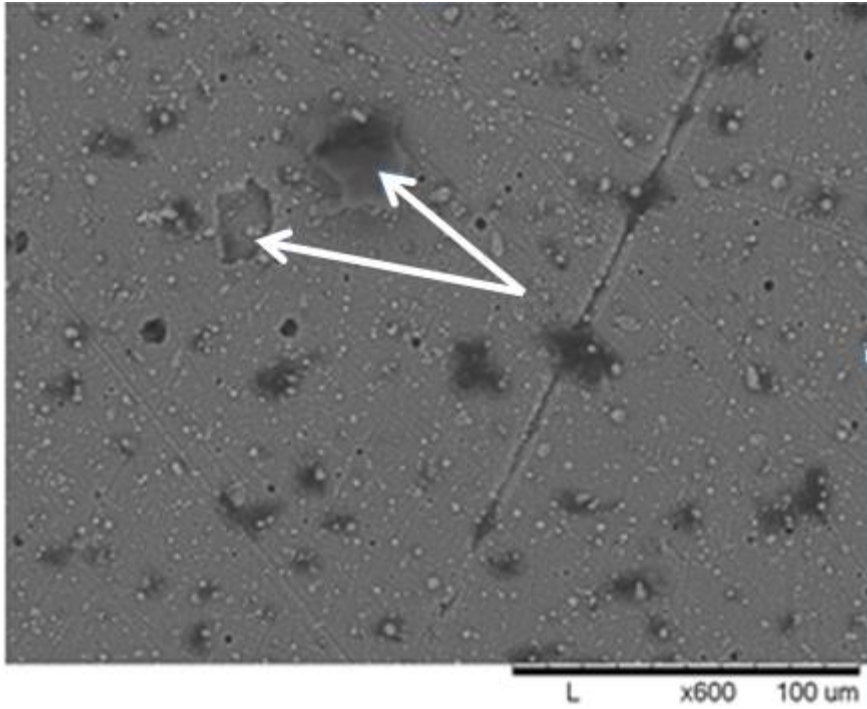


Figure 4.2: SEM micrograph showing: A nodule-detached crater (open void) on AlCrN coating surface

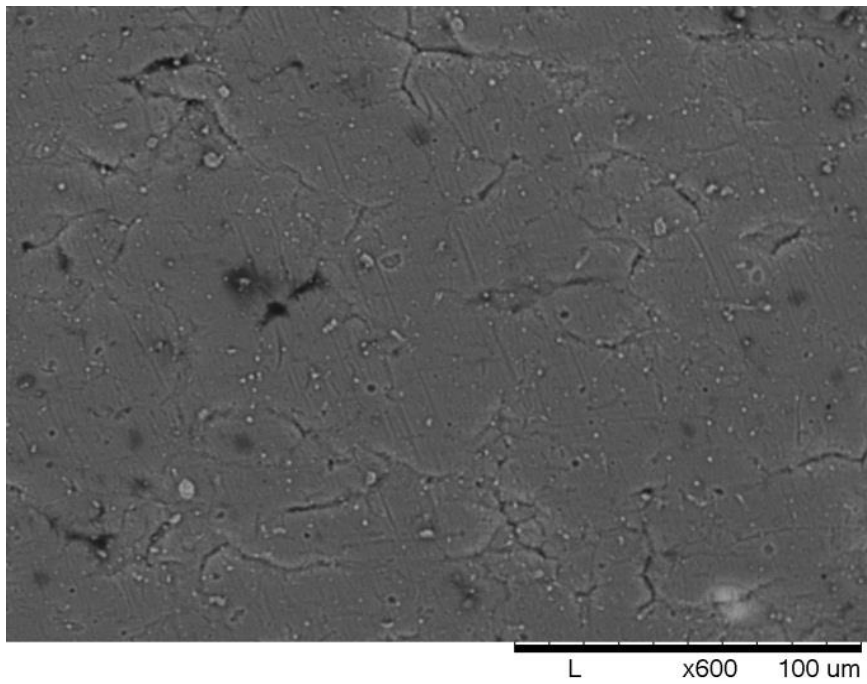


Figure 4.3: SEM image showing: Interconnected cracks on surface of TiAlN I coating

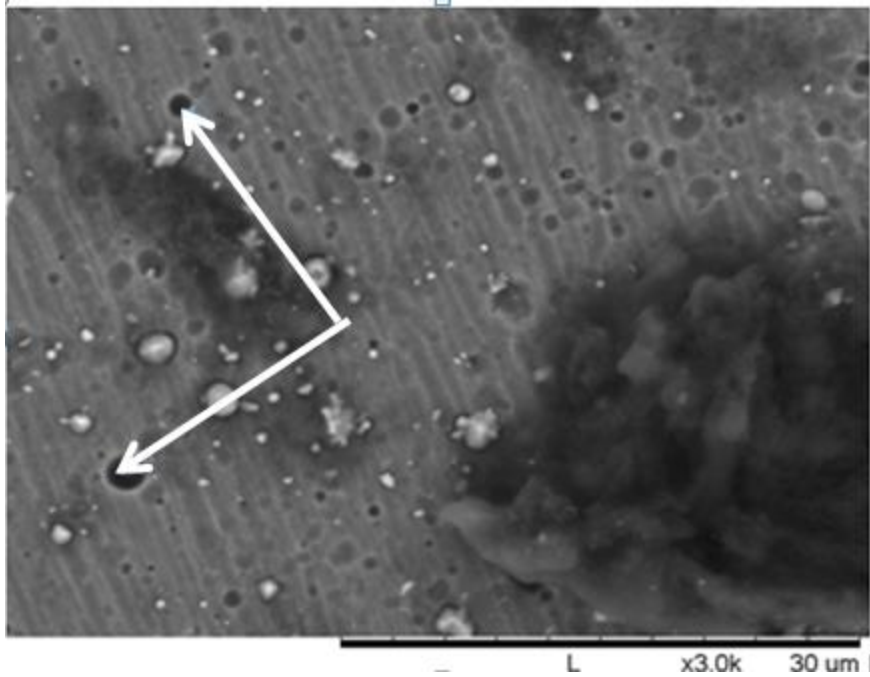


Figure 4.4: SEM Micrograph showing: Pinhole defect left by ejected particle on TiCN film.

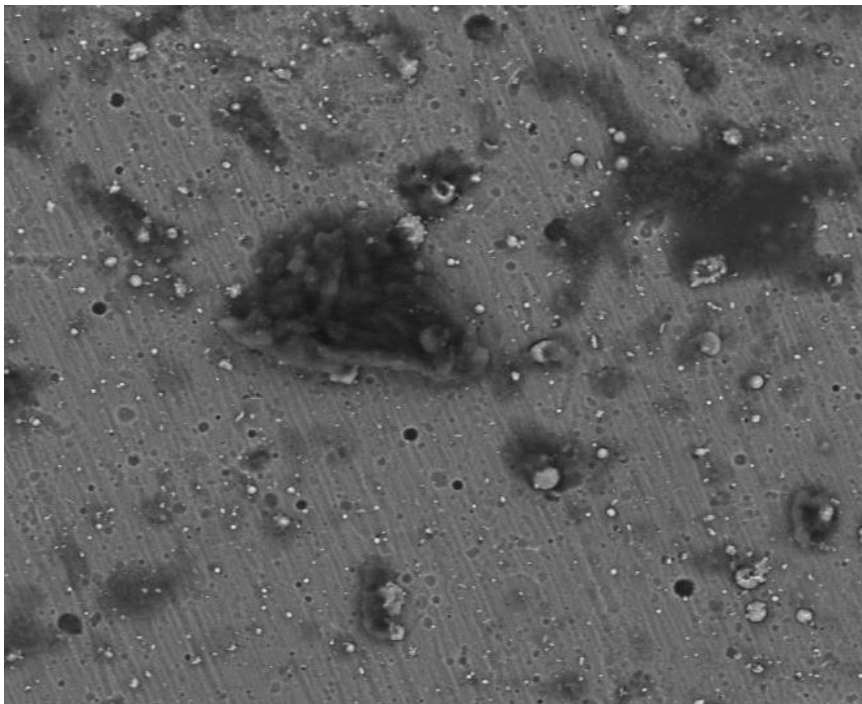


Figure 4.5: SEM micrograph showing: Large crater like defects on TiCN surface.

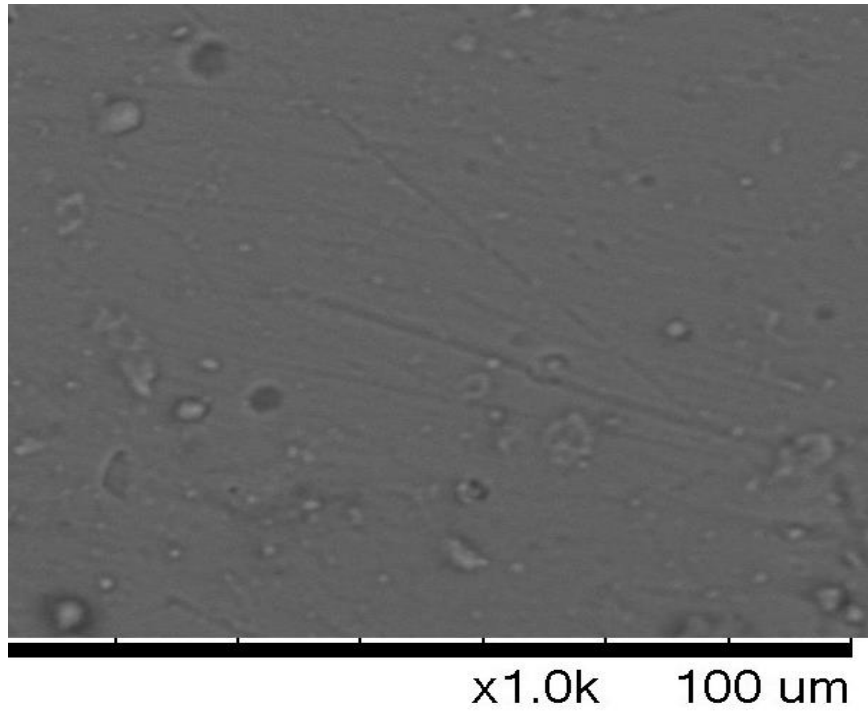


Figure 4.6: SEM micrograph of TiAlN II coating

4.1.3 Chemical Composition

EDS Analysis was used to characterize the chemical composition of the coatings and the AIS316L steel substrate.

4.2 Corrosion behavior of coatings

Potentiodynamic polarization measurements tests were conducted on the coatings to investigate their coating characteristics. The coatings were all deposited on AISI 316L steel substrate. The unprotected substrate was evaluated for corrosion behaviors, the influence of the coating microstructure and presence of defects on coating performance have been investigated. Tested samples were examined by SEM and EDS to detect their physical as well as chemical response to a corrosive environment. Changes to the surface morphology and chemical composition were evaluated after the corrosion tests. A 3.5% NaCl solution was used in simulating the corrosive environment.

4.2.1 Potentiodynamic Polarization Tests

The potentiodynamic polarization curves of the substrate and each coating (i.e. TiCN, TiAlN and AlCrN) in 3.5 % wt. NaCl are illustrated in Figure 4.6. The corresponding electrochemical parameters as deduced from the Tafel extrapolation polarization curves and calculations are presented in Table 4.2. They include the corrosion potential E_{corr} , current density i_{corr} , polarization resistance R_p , and Tafel slope β_a (anode), Tafel slope β_c (cathode). The protection efficiency and coating porosity have been evaluated quantitatively using Equation 3.3 and 3.4 respectively.

Table 4.2: Results of potentiodynamic polarization tests

Specimen	E_{corr} (V)	i_{corr} ($\mu\text{A}/\text{cm}^2$)	β_a (V/decade)	β_c (V/decade)	R_p ($\Omega \times 10^4 / \text{cm}^2$)	P_i (%)	P (%)
AISI 316L	-0.357	3.592	0.079	.147	1.24	-	-
TiCN	-0.185	0.0809	0.093	0.303	15.98	97.75	0.051
TiAlN I	-0.324	0.660	0.206	0.220	3.68	81.63	12.83
AlCrN	-0.169	0.9427	0.459	0.229	0.38	73.76	1.50
TiAlN II	-0.177	0.0474	0.159	0.354	52.70	98.68	0.012

The substrate has an E_{corr} of -0.357V in comparison to the coatings in which the corrosion potential is more positive (i.e., TiAlN = -0.324 V, TiAlN II = -0.177 V, TiCN = -0.185 V, AlCrN -0.169 V. Figure 4.10 illustrates a progressive shift in the corrosion potential of the coating from that of the substrate. According to [14], and [15] the shift to a more positive corrosion potential is indicative of a better corrosion resistance when compared to the uncoated substrate. This implies that despite the presence of defects, the coatings still offers protection to the substrate against corrosion. The result conforms to the study of [2] which

compared the electrochemical behavior of single layer CrN, TiAlN and TiN. It was noted that TiAlN exhibited the best corrosion resistance as compared to TiN and CrN. It has been reported that the incorporation of Aluminum generally results in better corrosion resistance [3]. In this study, two TiAlN samples with varying thickness were studied, the TiAlN coating with more thickness (TiAlN II (2.4 μ m)) exhibited better corrosion resistance and protection efficiency than all the other coatings. This corroborates the studies of Ş. Danişman and S. Savaş[16] and Jehn, H.A [60] which opined that increased thickness (below the critical thickness) of PVD hard coatings results in better corrosion resistance.

The uncoated AISI 316L steel substrate demonstrated a much larger corrosion current density as compared to the coatings. This corresponds to a higher corrosion rate. The TiAlN II showed the lowest corrosion current density, indicating the lowest corrosion rate and highest protective efficiency. Similarly, The TiCN film showed better protective capabilities than the AlCrN coating. The protective efficiency is in the order of TiAlN II > TiCN > TiAlN I > AlCrN (from best to worst), that is the thicker TiAlN coating had the highest corrosion protection efficiency.

As presented in the potentiodynamic polarization curves in Figure 4.7, all the three coatings improved the corrosion resistance as compared to the uncoated substrate. This is indicated by a lower passive current density of the substrate and a wider passive region.

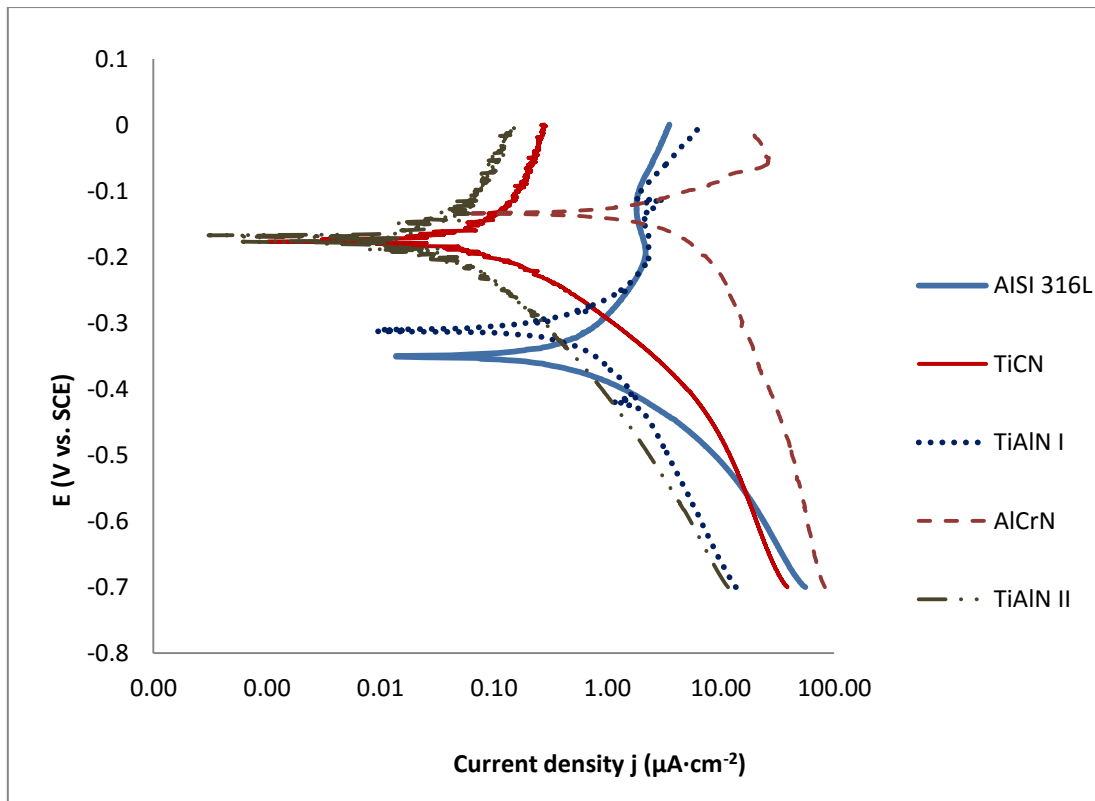


Figure 4.7: Potentiodynamic polarization curves of the substrate and coatings.

The chart of protective efficiency of the coatings and protective efficiency vs. polarization resistance of the substrate and coatings are presented in Figure 4.8 and Figure 4.9 respectively. It can be seen from Figure 4.8 that the polarization resistance is directly proportional to the corrosion efficiency.

In a coating/substrate system the corrosion density is an important indicator of the corrosion reactions that are occurring. It is a measurement of the ion exchange rate at the electrolyte-substrate in a unit area of the tested surface [1], a lower corrosion current density is an indication of a slower corrosion reaction which means a much slower corrosion rate. Coating samples with lower porosity values also have lower corrosion current densities but larger polarization resistance. This means they have better corrosion prevention abilities as expressed by the protective efficiency; this gives a strong indication of a correlation between porosities (which is a measure of defect density) in a coating and its corrosion behaviors.

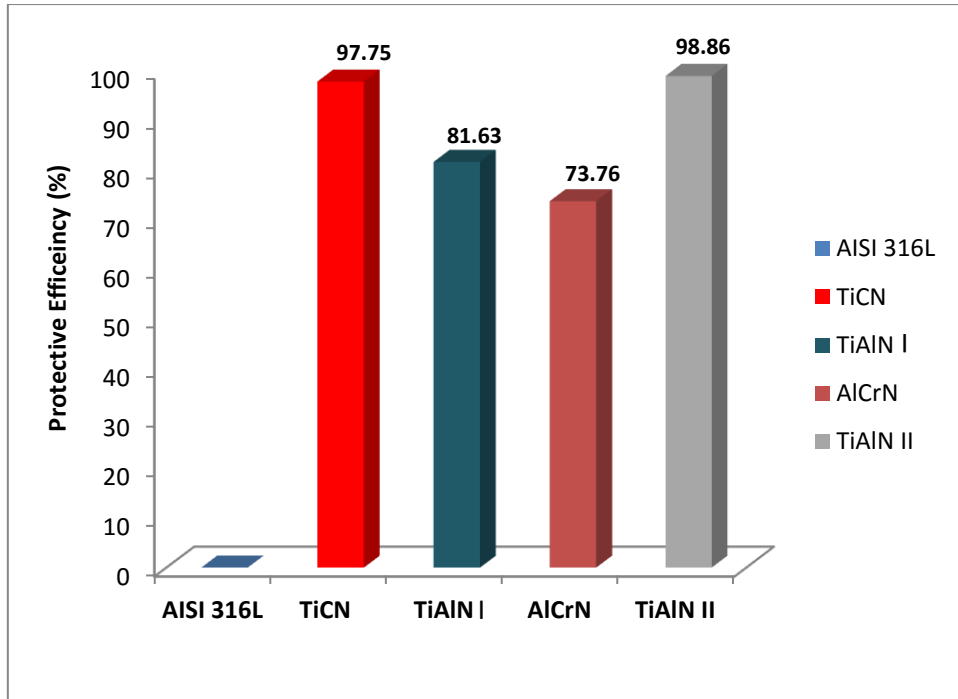


Figure 4.8: Protective efficiency of coatings

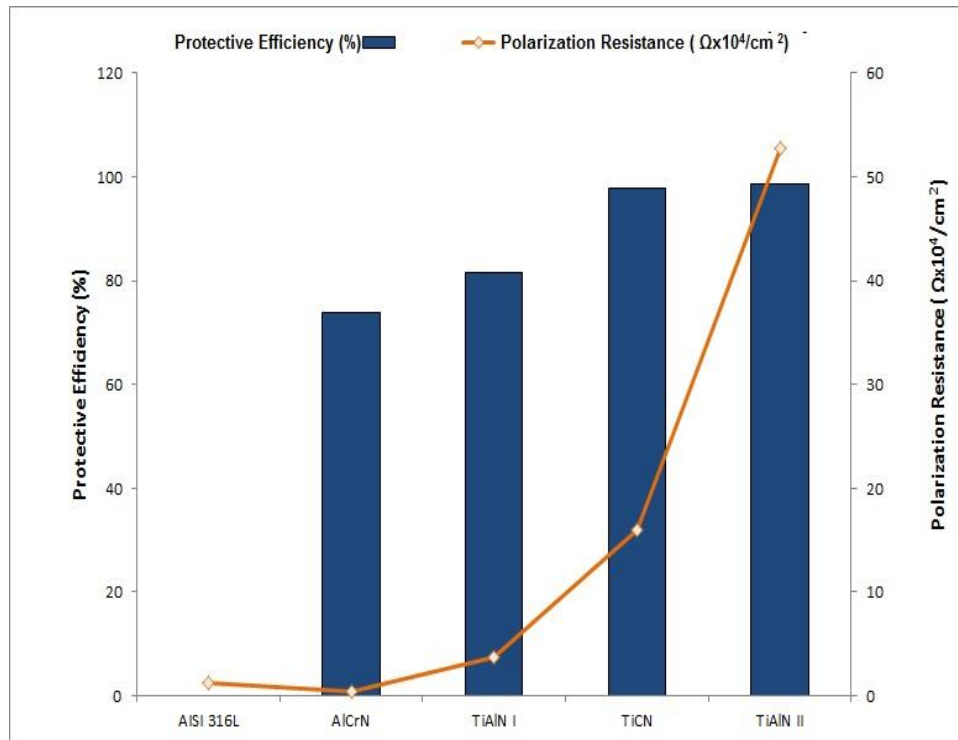


Figure 4.9: Protective efficiency and polarization resistance of the substrate and coatings.

The porosity of the coating is an important parameter in assessing the coating integrity. The higher the coefficient of porosity a coating, the higher the surface defect density [34]. The

porosity of the coatings as calculated from Equation 3.4 is presented in Table 4.2 . It can be noted that the porosity is directly related to the protection efficiency of the coating. The TiAlN II sample with the lowest porosity of 0.012 % showed the highest protective efficiency of 98.68 %, the coating also has the highest polarization resistance and smallest corrosion current density. Conversely, the TiAlN still had better protective efficiency than the AlCrN despite its increased porosity. This may be due to the nature of defect associated with the different coatings.

The corrosion rate is proportional to the i_{corr} , it is regarded as a critical factor in evaluating the kinetics of a corrosion process. The corrosion density can be determined by equation 4.1: The corrosion resistance is directly proportional to the i_{corr} [19]. L. According to Zhang *et al* [19], [3], and [2] a significant decrease in the corrosion density of the coatings in comparison with substrate is indicative that they can all serve as a protective barrier between the substrate and the corrosive electrolyte. The corrosion current density of the steel substrate was 3.592 $\mu\text{A}/\text{cm}^2$ while the TiAlN II coatings with the lowest i_{corr} possess the highest corrosion resistance as determined by its protective efficiency of 98.68 %. The sample also indicated the lowest porosity. This is consistent with various studies (such as [19] [3] and [2]) where the porosity where samples with lowest porosities, lowest corrosion current density and highest polarization potentials indicated the best protective efficiencies. The corrosion current densities are illustrated in Figure 2.11, the value clearly shows a significant decrease for the coatings.

The corrosion current density can be evaluated from:

$$i_{corr} = \frac{I_{corr}}{A} \quad 4.1$$

where:

- i_{corr} corrosion Density, $\mu\text{A}/\text{cm}^2$;
- I_{corr} total anodic current, A,
- A exposed specimen area, cm^2 .

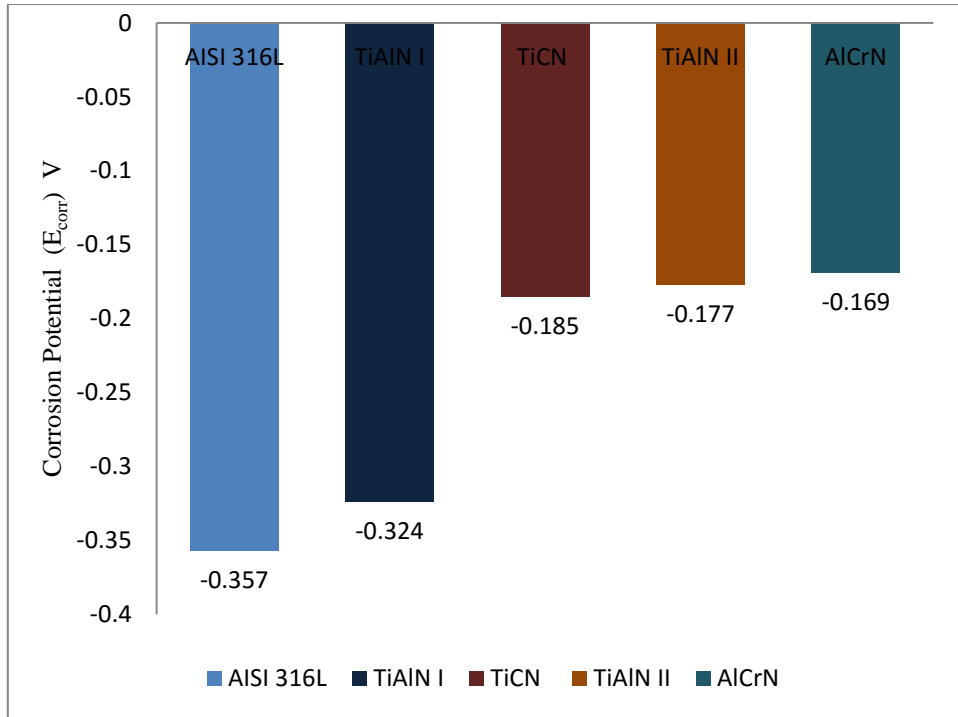


Figure 4.10: Corrosion Potential of Substrate and Coatings

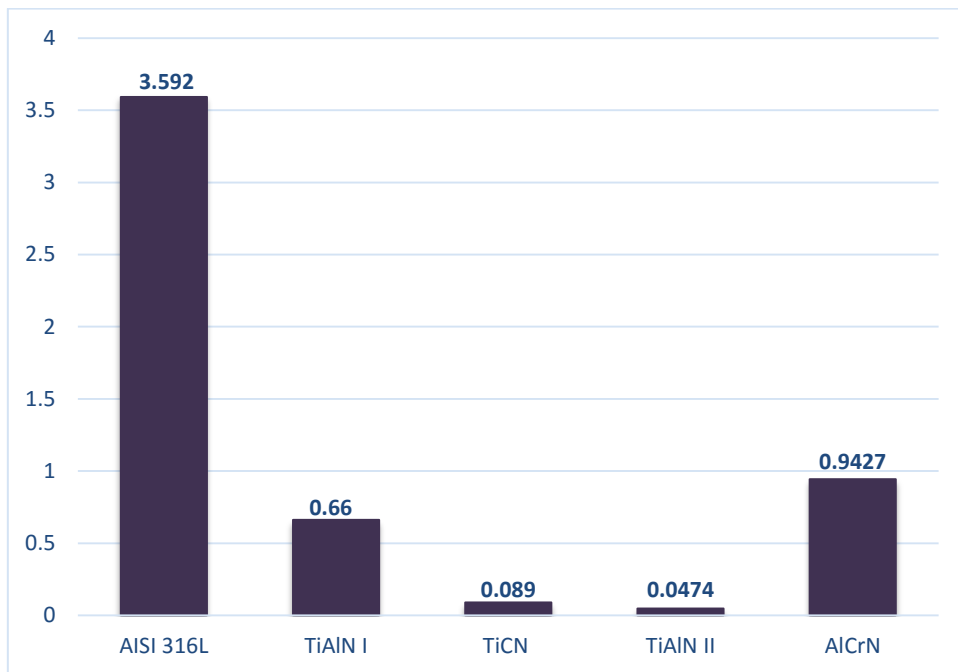


Figure 4.11: Corrosion current density i_{corr} ($\mu\text{A}/\text{cm}^2$) of the coatings and substrate.

5 Conclusions

TiCN, TiAlN and AlCrN coatings have been successfully deposited on AISI 316L steel substrate by a Platin π^{80} system under a reactive nitrogen atmosphere using Lateral Rotating ARC-Cathodes (LARC) technology. The microstructure and morphologies as well as the electrochemical properties of the coatings have been successfully evaluated by SEM and potentiodynamic polarization measurements.

All the coatings have been found to have very low porosities except the TiAlN I with 12.83 % porosity. The corrosion current densities of all the coatings in an aerated 3.5 wt. % NaCl were considerably lower than that of the steel substrate. From the electrochemical data, the porosity and protective efficiencies of the coatings have been calculated. The following conclusions can be obtained from this study:

- 1) The TiAlN II (the thicker TiAlN (2.4 μm)) displayed the highest corrosion resistance, the lowest porosity (0.012 %) and the best protective efficiency of 98.68 %. The coating also showed the lowest corrosion current density of $0.0474\mu\text{A}/\text{cm}^2$ and highest polarization resistance of $5.27\text{ k}\Omega/\text{cm}^2$.
- 2) The corrosion resistance is in the following order (from the best to the worst) TiAlN II (98.68%) > TiCN 97.75 % > TiAlN I (81.63 %) > AlCrN (73.76 %). Similarly, the porosity was in the same order except for TiAlN I which had better protection efficiency than the AlCrN despite having a worse porosity coefficient. The measured porosity is in the following order: (from the highest to the lowest i.e. worst to best): TiAlN (12.83 %) < AlCrN (1.50 %) < TiCN (0.051 %) < TiAlN II (0.012 %).
- 3) The porosity of the coating which is a measure of the defect density directly influences the corrosion resistance as measured from the protective efficiency. The protective efficiency increases with decreasing porosity.
- 4) It can be deduced that all the coatings served as protective barrier on the substrate against the corrosive media. They posed an improved corrosion resistance despite the presence of defects.

References

- [1] F. Cai, *Tribological and Electrochemical Corrosion Behaviours of Titanium Nitride and Chromium Nitride Based PVD Coating Systems*, no. April. 2011.
- [2] V. K. William Grips, H. C. Barshilia, V. E. Selvi, and K. S. Rajam, "Electrochemical behavior of single layer CrN, TiN, TiAlN coatings and nanolayered TiAlN/CrN multilayer coatings prepared by reactive direct current magnetron sputtering," *Thin Solid Films*, vol. 514, no. 1–2, pp. 204–211, Aug. 2006.
- [3] Y. H. Yoo, D. P. Le, J. G. Kim, S. K. Kim, and P. Van Vinh, "Corrosion behavior of TiN, TiAlN, TiAlSiN thin films deposited on tool steel in the 3.5 wt.% NaCl solution," *Thin Solid Films*, vol. 516, no. 11, pp. 3544–3548, Apr. 2008.
- [4] P. Panjan, M. Čekada, M. Panjan, and D. Kek-Merl, "Growth defects in PVD hard coatings," *Vacuum*, vol. 84, no. 1, pp. 209–214, 2009.
- [5] U. K. Chatterjee, S. K. Bose, and S. K. Roy, *Environmental Degradation of Metals: Corrosion Technology Series/14*. CRC Press, 2001.
- [6] S. Zhang, H. L. Wang, S.-E. Ong, D. Sun, and X. L. Bui, "Hard yet Tough Nanocomposite Coatings – Present Status and Future Trends," *Plasma Process. Polym.*, vol. 4, no. 3, pp. 219–228, 2007.
- [7] M. A. AL-Bukhaiti, K. A. Al-hatab, W. Tillmann, F. Hoffmann, and T. Sprute, "Tribological and mechanical properties of Ti/TiAlN/TiAlCN nanoscale multilayer PVD coatings deposited on AISI H11 hot work tool steel," *Appl. Surf. Sci.*, vol. 318, pp. 180–190, Nov. 2014.
- [8] "Tribological characterization of selected hard coatings," 2009.
- [9] F. C. Walsh, C. Ponce de León, C. Kerr, S. Court, and B. D. Barker, "Electrochemical characterisation of the porosity and corrosion resistance of electrochemically deposited metal coatings," *Surf. Coatings Technol.*, vol. 202, no. 21, pp. 5092–5102, Jul. 2008.
- [10] B. Bhushan and B. K. Gupta, *Handbook of tribology: materials, coatings, and surface treatments*. McGraw-Hill, 1991.
- [11] *Wear: Materials, Mechanisms and Practice*. John Wiley & Sons, 2006.
- [12] K. Adachi, K. Kato, and N. Chen, "Wear map of ceramics," *Wear*, vol. 203–204, pp.

- 291–301, Mar. 1997.
- [13] E. Bardal, *Corrosion and Protection*. Springer Science & Business Media, 2007.
- [14] N. Perez, *Electrochemistry and Corrosion Science*. Springer Science & Business Media, 2004.
- [15] S. D. Cramer and B. S. Covino, “ASM Handbook Vol. 13a: Corrosion - Fundamentals, Testing, and Protection,” *Asm*, vol. 13, p. 1135, 2003.
- [16] E. Faculty, “The Effect of Ceramic Coatings on Corrosion and Wear Behaviour,” *Wear*, vol. 27, no. 3, pp. 41–48, 2005.
- [17] F. Lang and Z. Yu, “The corrosion resistance and wear resistance of thick TiN coatings deposited by arc ion plating,” *Surf. Coatings Technol.*, vol. 145, no. 1–3, pp. 80–87, 2001.
- [18] V. Chawla, A. Chawla, Y. Mehta, D. Puri, S. Prakash, and B. S. Sidhu, “Investigation of properties and corrosion behavior of hard TiAlN and AlCrN PVD thin coatings in the 3 wt % NaCl solution,” vol. 47, pp. 48–55, 2011.
- [19] L. Zhang, Y. Chen, Y. P. Feng, S. Chen, Q. L. Wan, and J. F. Zhu, “Electrochemical characterization of AlTiN, AlCrN and AlCrSiWN coatings,” *Int. J. Refract. Met. Hard Mater.*, vol. 53, pp. 68–73, 2015.
- [20] X. zhao Ding, A. L. K. Tan, X. T. Zeng, C. Wang, T. Yue, and C. Q. Sun, “Corrosion resistance of CrAlN and TiAlN coatings deposited by lateral rotating cathode arc,” *Thin Solid Films*, vol. 516, no. 16, pp. 5716–5720, 2008.
- [21] X. zhao Ding, X. T. Zeng, Y. C. Liu, F. Z. Fang, and G. C. Lim, “Cr_{1-x}Al_xN coatings deposited by lateral rotating cathode arc for high speed machining applications,” *Thin Solid Films*, vol. 516, no. 8, pp. 1710–1715, 2008.
- [22] “Electrochemical Corrosion Measurements-Galvanic Corrosion.” [Online]. Available: <http://www.gamry.com/application-notes/corrosion-coatings/basics-of-electrochemical-corrosion-measurements/>. [Accessed: 17-May-2016].
- [23] S. N. Lvov, *Introduction to Electrochemical Science and Engineering*. CRC Press, 2014.
- [24] *Corrosion Tests and Standards*. ASTM International.

- [25] Autolab Application Note EC08, “Basic overview of the working principle of a potentiostat/galvanostat (PGSTAT) – Electrochemical cell setup,” *Metrohm Autolab.B.V*, pp. 1–3, 2011.
- [26] M. Stern and A. L. Geaby, “Electrochemical Polarization,” *J. Electrochem. Soc.*, vol. 104, no. 1, p. 56, Jan. 1957.
- [27] M. Cekada, P. Panjan, D. Kek-Merl, M. Panjan, and G. Kapun, “SEM study of defects in PVD hard coatings,” *Vacuum*, vol. 82, no. 2 SPEC. ISS., pp. 252–256, Oct. 2007.
- [28] P. Panjan, M. Čekada, M. Panjan, D. Kek-Merl, F. Zupanič, L. Čurković, and S. Paskvale, “Surface density of growth defects in different PVD hard coatings prepared by sputtering,” *Vacuum*, vol. 86, no. 6, pp. 794–798, Jan. 2012.
- [29] P. Panjan, D. Kek Merl, F. Zupanič, M. Čekada, and M. Panjan, “SEM study of defects in PVD hard coatings using focused ion beam milling,” *Surf. Coatings Technol.*, vol. 202, no. 11, pp. 2302–2305, Feb. 2008.
- [30] P. Gselman, T. Boncina, F. Zupanic, P. Panjan, D. K. Merl, and M. Cekada, “Characterization of defects in PVD TiAlN hard coatings,” *Mater. Technol.*, vol. 46, no. 4, pp. 351–354, 2012.
- [31] P. Panjan, P. Gselman, D. Kek-Merl, M. Čekada, M. Panjan, G. Dražić, T. Bončina, and F. Zupanič, “Growth defect density in PVD hard coatings prepared by different deposition techniques,” *Surf. Coatings Technol.*, vol. 237, pp. 349–356, Dec. 2013.
- [32] A. Drnovšek, P. Panjan, M. Panjan, and M. Čekada, “The influence of growth defects in sputter-deposited TiAlN hard coatings on their tribological behavior,” *Surf. Coatings Technol.*, vol. 288, pp. 171–178, Feb. 2016.
- [33] P. Panjan, M. Čekada, M. Panjan, and D. Kek-Merl, “Growth defects in PVD hard coatings,” *Vacuum*, vol. 84, no. 1, pp. 209–214, Aug. 2009.
- [34] D. K. Merl, P. Panjan, M. Panjan, and M. Čekada, “The role of surface defects density on corrosion resistance of PVD hard coatings,” *Plasma Process. Polym.*, vol. 4, no. SUPPL.1, pp. 613–617, 2007.
- [35] C. He, J. Zhang, J. Wang, G. Ma, D. Zhao, and Q. Cai, “Effect of structural defects on corrosion initiation of TiN nanocrystalline films,” *Appl. Surf. Sci.*, vol. 276, pp. 667–671, Jul. 2013.

- [36] L. Ning, “Nano-multilayered Self-adaptive Hard PVD Coatings for Dry High Performance Machining,” p. 218, 1014.
- [37] *High Temperature Materials and Mechanisms*. CRC Press, 2014.
- [38] “physical vapour deposition (PVD).” [Online]. Available: <http://www.metaux.ulg.ac.be/metaux/index.php?page=nanomateriaux>. [Accessed: 03-May-2016].
- [39] L. SHAN, Y. ZHANG, Y. WANG, J. LI, X. JIANG, and J. CHEN, “Corrosion and wear behaviors of PVD CrN and CrSiN coatings in seawater,” *Trans. Nonferrous Met. Soc. China*, vol. 26, no. 1, pp. 175–184, Jan. 2016.
- [40] V. K. W. Grips, V. Ezhil Selvi, H. C. Barshilia, and K. S. Rajam, “Effect of electroless nickel interlayer on the electrochemical behavior of single layer CrN, TiN, TiAlN coatings and nanolayered TiAlN/CrN multilayer coatings prepared by reactive dc magnetron sputtering,” *Electrochim. Acta*, vol. 51, no. 17, pp. 3461–3468, 2006.
- [41] Y. C. Chim, X. Z. Ding, X. T. Zeng, and S. Zhang, “Oxidation resistance of TiN, CrN, TiAlN and CrAlN coatings deposited by lateral rotating cathode arc,” *Thin Solid Films*, vol. 517, no. 17, pp. 4845–4849, Jul. 2009.
- [42] Z. Xu, Z. Wang, G. Huang, R. Mu, and L. He, “Morphology, bond strength and thermal cycling behavior of (Ni, Pt)Al/YSZ EB-PVD thermal barrier coatings,” *J. Alloys Compd.*, vol. 651, pp. 445–453, Dec. 2015.
- [43] T. Leyendecker, O. Lemmer, S. Esser, and J. Ebberink, “The development of the PVD coating TiAlN as a commercial coating for cutting tools,” *Surf. Coatings Technol.*, vol. 48, no. 2, pp. 175–178, Nov. 1991.
- [44] J. L. Mo, M. H. Zhu, B. Lei, Y. X. Leng, and N. Huang, “Comparison of tribological behaviours of AlCrN and TiAlN coatings—Deposited by physical vapor deposition,” *Wear*, vol. 263, no. 7–12, pp. 1423–1429, Sep. 2007.
- [45] F. Hollstein and P. Louda, “Bio-compatible low reflective coatings for surgical tools using reactive d.c.-magnetron sputtering and arc evaporation - a comparison regarding steam sterilization resistance and nickel diffusion,” *Surf. Coatings Technol.*, vol. 120–121, pp. 672–681, 1999.
- [46] T. Polcar, T. Kubart, R. Novák, L. Kopecký, and P. Široký, “Comparison of

- tribological behaviour of TiN, TiCN and CrN at elevated temperatures,” *Surf. Coatings Technol.*, vol. 193, no. 1–3, pp. 192–199, Apr. 2005.
- [47] P. . Jindal, A. . Santhanam, U. Schleinkofer, and A. . Shuster, “Performance of PVD TiN, TiCN, and TiAlN coated cemented carbide tools in turning,” *Int. J. Refract. Met. Hard Mater.*, vol. 17, no. 1–3, pp. 163–170, May 1999.
- [48] V. Braic, M. Braic, M. Balaceanu, A. Vladescu, C. N. Zoita, I. Titorencu, and V. Jinga, “(Zr,Ti)CN coatings as potential candidates for biomedical applications,” *Surf. Coatings Technol.*, vol. 206, no. 4, pp. 604–609, Nov. 2011.
- [49] K. Feng, G. Wu, Z. Li, X. Cai, and P. K. Chu, “Corrosion behavior of SS316L in simulated and accelerated PEMFC environments,” *Int. J. Hydrogen Energy*, vol. 36, no. 20, pp. 13032–13042, 2011.
- [50] S. Anders, S. Raoux, K. Krishnan, R. A. MacGill, and I. G. Brown, “Plasma distribution of cathodic arc deposition systems,” *J. Appl. Phys.*, vol. 79, no. 9, pp. 6785–6790, 1996.
- [51] P. L. Sun, C. H. Hsu, S. H. Liu, C. Y. Su, and C. K. Lin, “Analysis on microstructure and characteristics of TiAlN/CrN nano-multilayer films deposited by cathodic arc deposition,” *Thin Solid Films*, vol. 518, no. 24, pp. 7519–7522, 2010.
- [52] M. Jilek, T. Cselle, P. Holubar, M. Morstein, M. G. J. Veprek-Heijman, and S. Veprek, “Development of novel coating technology by vacuum arc with rotating cathodes for industrial production of nc-(Al_{1-x}Ti_x)N/a- Si₃N₄ superhard nanocomposite coatings for dry, hard machining,” *Plasma Chem. Plasma Process.*, vol. 24, no. 4, pp. 493–510, 2004.
- [53] D. G. Enos and L. L. Scribner, “The Potentiodynamic Polarization Scan Technical Report 33,” *Cent. Electrochem. Sci. Eng.*, pp. 1–13, 1997.
- [54] J. Creus, A. Billard, and F. Sanchette, “Corrosion behaviour of amorphous Al-Cr and Al-Cr-(N) coatings deposited by dc magnetron sputtering on mild steel substrate,” *Thin Solid Films*, vol. 466, no. 1–2, pp. 1–9, Nov. 2004.
- [55] H. . Wang, M. . Stack, S. . Lyon, P. Hovsepian, and W.-D. Münz, “The corrosion behaviour of macroparticle defects in arc bond-sputtered CrN/NbN superlattice coatings,” *Surf. Coatings Technol.*, vol. 126, no. 2–3, pp. 279–287, Apr. 2000.

- [56] C. Liu, Q. Bi, A. Leyland, and A. Matthews, "An electrochemical impedance spectroscopy study of the corrosion behavior of PVD coated steels in 0.5 N NaCl aqueous solution: Part II. EIS interpretation of corrosion behaviour," *Corros. Sci.*, vol. 45, no. 6, pp. 1257–1273, Jun. 2003.
- [57] J. Creus, H. Mazille, and H. Idrissi, "Porosity evaluation of protective coatings onto steel, through electrochemical techniques," *Surf. Coatings Technol.*, vol. 130, no. 2–3, pp. 224–232, Aug. 2000.
- [58] B. Matthes, E. Broszeit, J. Aromaa, H. Ronkainen, S. P. Hannula, A. Leyland, and A. Matthews, "Corrosion performance of some titanium-based hard coatings," *Surf. Coatings Technol.*, vol. 49, no. 1–3, pp. 489–495, Dec. 1991.
- [59] R. Kossowsky, *Surface Modeling Engineering, Volume 1*. CRC Press, 1989.
- [60] H. A. Jehn, "Improvement of the corrosion resistance of PVD hard coating–substrate systems," *Surf. Coatings Technol.*, vol. 125, no. 1–3, pp. 212–217, Mar. 2000.

